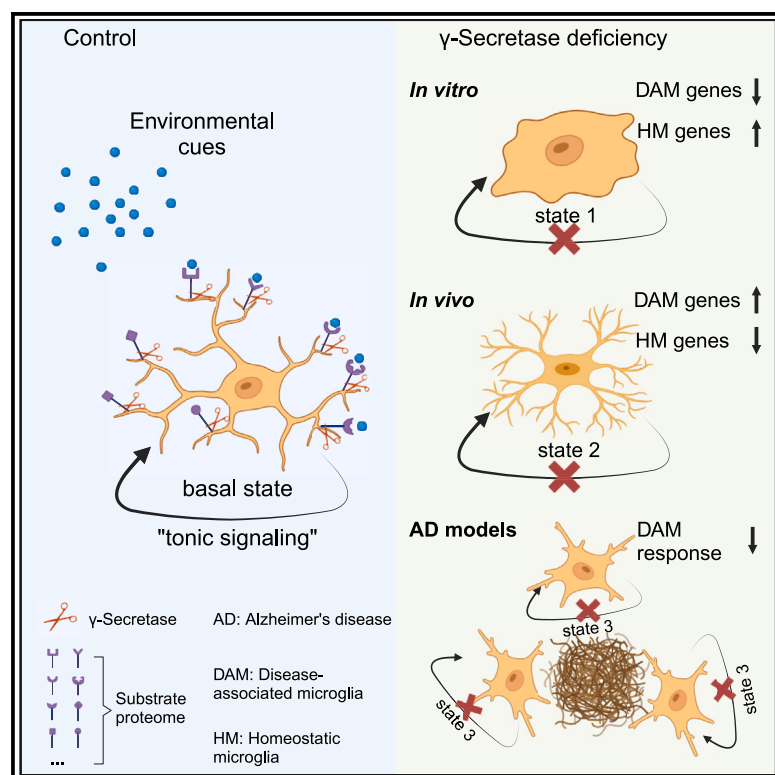# The γ-secretase substrate proteome and its role in cell signaling regulation

Graphical abstract

Authors

Pengfei Hou, Magdalena Zielonka, Lutgarde Serneels, ..., Renzo Mancuso, Andrew J.M. Howden, Bart De Strooper

Correspondence

bart.destrooper@kuleuven.be

In brief

The field has been lacking an unbiased approach for large-scale endogenous γ-secretase substrate identification. Hou et al. report a G-SECSI method and demonstrate that the γ-secretase substrate proteome is intimately connected to the intracellular signaling in microglia. γ-Secretase deficiency has profound effects on microglia in response to amyloid pathology.

Highlights

- G-SECSI: an unbiased approach for γ-secretase substrate identification

- γ-Secretase substrates are central in intracellular microglial signaling

- γ-Secretase maintains the basal states of *in vitro* and *in vivo* microglia models

- γ-Secretase deficiency impedes disease-associated microglia (DAM) response

CellPress

Article

The γ-secretase substrate proteome and its role in cell signaling regulation

Pengfei Hou,[1,2,10] Magdalena Zielonka,[1,2,10] Lutgarde Serneels,[1,2] Anna Martinez-Muriana,[1,2] Nicola Fattorelli,[1,2] Leen Wolfs,[1,2] Suresh Poovathingal,[2,3] Dries T'Syen,[1,2] Sriram Balusu,[1,2] Tom Theys,[4] Mark Fiers,[1,2,5,6] Renzo Mancuso,[7,8] Andrew J.M. Howden,[9] and Bart De Strooper[1,2,5,6,11,*]

[1]Laboratory for the Research of Neurodegenerative Diseases, VIB Center for Brain & Disease Research, VIB, Leuven 3000, Belgium
[2]Department of Neurosciences and Leuven Brain Institute, KU Leuven, Leuven 3000, Belgium
[3]Single Cell & Microfluidics Expertise Unit, VIB Center for Brain & Disease Research, VIB, Leuven 3000, Belgium
[4]Department of Neurosciences, Research Group Experimental Neurosurgery and Neuroanatomy, KU Leuven, Leuven 3000, Belgium
[5]Center for Human Genetics, KU Leuven, Leuven 3000, Belgium
[6]Dementia Research Institute, Institute of Neurology, University College London, London WC1E 6BT, UK
[7]Microglia and Inflammation in Neurological Disorders (MIND) Lab, VIB Center for Molecular Neurology, VIB, Antwerp 2610, Belgium
[8]Department of Biomedical Sciences, University of Antwerp, Antwerp 2610, Belgium
[9]Division of Cell Signaling and Immunology, School of Life Sciences, University of Dundee, Dundee DD1 4HN, UK
[10]These authors contributed equally
[11]Lead contact
*Correspondence: bart.destrooper@kuleuven.be
https://doi.org/10.1016/j.molcel.2023.10.029

SUMMARY

γ-Secretases mediate the regulated intramembrane proteolysis (RIP) of more than 150 integral membrane proteins. We developed an unbiased γ-secretase substrate identification (G-SECSI) method to study to what extent these proteins are processed in parallel. We demonstrate here parallel processing of at least 85 membrane proteins in human microglia in steady-state cell culture conditions. Pharmacological inhibition of γ-secretase caused substantial changes of human microglial transcriptomes, including the expression of genes related to the disease-associated microglia (DAM) response described in Alzheimer disease (AD). While the overall effects of γ-secretase deficiency on transcriptomic cell states remained limited in control conditions, exposure of mouse microglia to AD-inducing amyloid plaques strongly blocked their capacity to mount this putatively protective DAM cell state. We conclude that γ-secretase serves as a critical signaling hub integrating the effects of multiple extracellular stimuli into the overall transcriptome of the cell.
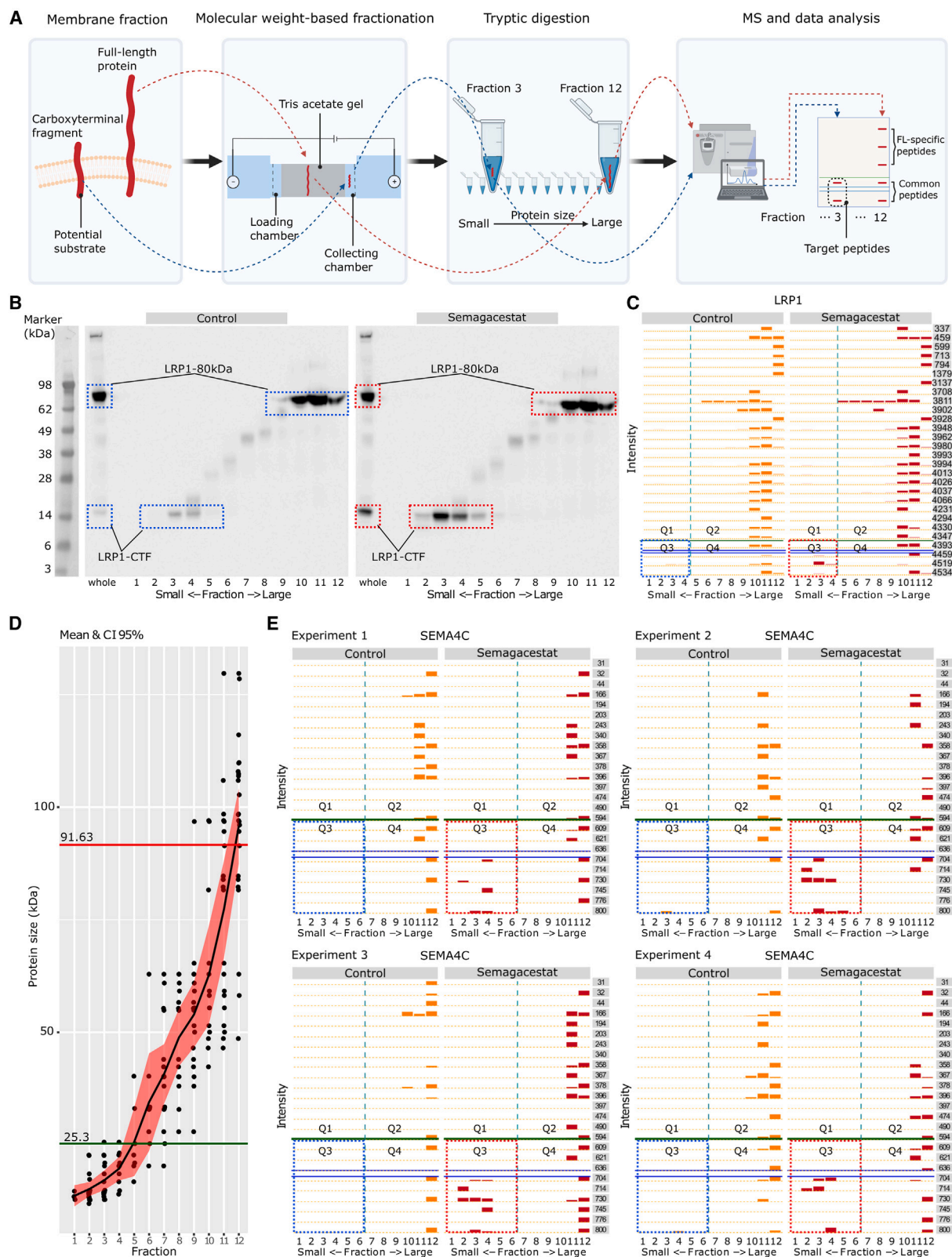
INTRODUCTION

γ-Secretase activity is mediated by a family of four intramembranous tetrameric proteases,[1,2] which cleaves a wide range of integral membrane proteins, for instance, the amyloid precursor protein (APP) in Alzheimer disease (AD)[3] and Notch in development and cancer.[4,5] During this process, the intracellular domains of the substrates are released. Many of these appear to regulate cell signaling.[6] Similar signaling is performed by other intramembranous proteases such as the rhomboids or S2P and was baptized "regulated intramembrane proteolysis (RIP)".[7] Most importantly, signaling mediated by RIP is irreversible, in contrast to other signaling mechanisms like phosphorylation.[6]

Despite evidence for the role of γ-secretases in intracellular signaling, clearing membrane-bound protein stubs generated by ectodomain shedding is the other main task of γ-secretase function.[8] γ-Secretases have the property to trim their substrates in the membrane, removing hydrophobic amino acids, re-

sulting ultimately in the release of small peptides into the extracellular milieu.[9] The function of many of these peptides remains unknown, but one peptide of note is the Aβ peptide cleaved from APP.[3] Aβ has important pathological relevance in the context of AD.

Most studies on the biology and pharmacology of γ-secretases focus on analyzing the intracellular signaling of one specific substrate at a time.[10] For example, γ-secretase limits the inflammatory response through the processing of LRP1,[11] whereas γ-secretase cleavage of SIRPα enhances inflammatory signaling.[12] These studies have led to important insights into the function of different substrates, but they do not really tackle the question of the physiological function of the protease itself. This would require the determination of the total substrate proteome in each experimental condition. However, mass spectrometry (MS) cannot discriminate full-length (FL) unprocessed precursors from accumulating substrates, hampering the development of an unbiased approach. Studies of γ-secretase substrates therefore have been largely limited to known proteins for which

A Membrane fraction | Molecular weight-based fractionation | Tryptic digestion | MS and data analysis

B (Western blot — Control and Semagacestat, Marker kDa: 98, 62, 49, 38, 28, 14, 6, 3; LRP1-80kDa, LRP1-CTF; whole, fractions 1–12, Small ←Fraction→ Large)

C LRP1 (Control and Semagacestat intensity plots, fractions 1–12, Small ←Fraction→ Large)

D Mean & CI 95% (Protein size (kDa) vs Fraction; 91.63, 25.3)

E Experiment 1 SEMA4C, Experiment 2 SEMA4C, Experiment 3 SEMA4C, Experiment 4 SEMA4C (Control and Semagacestat intensity plots)

(legend on next page)

antibodies are available or in which epitope tags were engineered.[10]

Progress in other fields of intramembrane proteolysis illustrates the importance of unbiased approaches to understand the role(s) of these proteases. An elegant method directly links serine or cysteine proteases to their substrates by introducing a 2,3-diaminopropionic acid (Dap) substitution into the catalytic site, enabling the formation of a hydrolysis-resistant substrate-enzyme intermediate through a stable amide bond.[13,14] The enzyme-substrate complexes can be recovered and analyzed by MS. Substrates of the intramembrane cleaving rhomboid RHBDL4 were identified, demonstrating its role in non-canonical secretion of endoplasmic reticulum-resident chaperones.[15] However, aspartyl proteases use their catalytic aspartate residues to interact with water, and the carbonyl oxygen of the scissile amide bond does not involve the formation of an acyl-enzyme intermediate.[16] Therefore, this approach is not applicable for the identification of γ-secretase substrates.

In silico approaches are another way to unbiasedly identify substrates for intramembrane cleaving proteases, illustrated by a study of the signal peptidase complex (SPC).[17] SPC is a family of membrane-integral serine proteases whose canonical role is to cleave off N-terminal signal peptides.[18] Surveying the human proteome for the presence of a specific Ala-X-Ala motif characteristic for the cleavage sites of SPC,[19] candidate cleavage sites were found in 1,297 membrane proteins but in regions outside of the canonical site at the N terminus.[17,20] Subsequent validation experiments showed that SPC can cleave those sites when they become exposed because of protein misfolding.[17] Thus, this study revealed an unexpected degradation function of SPC in addition to its well-known signaling function.[18] Unlike SPC, γ-secretase substrates do not share such easily identifiable consensus cleavage sequences,[10,21,22] making prediction of their substrates unreliable. Artificial intelligence methods linking sequence features with predicted conformational structures might provide a solution,[23] but direct experimental identification of substrates using unbiased screening approaches will be important to support such analysis.

We selected microglial cells as a relevant and intriguing model system to study the role of γ-secretases in a systemic way. Microglia are resident macrophages of the central nervous system (CNS), which constantly survey the brain parenchyma.[24,25] They play a protective role in maintaining brain homeostasis but may act in a detrimental way in AD and other brain disorders.[26–29] Several genes involved in microglial cell fate determination encode γ-secretase substrates, for instance, CSF1R is vital for microglial survival[30] and is highly expressed in "homeostatic" (HM) microglia, while AXL is responsible for microglial phagocytosis of Aβ plaques[31] and is highly expressed in disease-associated microglia (DAM). Another known substrate of γ-secretase in microglia is TREM2,[32] which carries major genetic risk of AD.[33,34] TREM2 is of pivotal importance in the DAM response of microglia to amyloid plaques, and deleting *Trem2* causes a blockage of this putatively protective microglial response.[35–37]

We analyzed the γ-secretase substrate proteome in human H9 ESC-derived microglia-like cells (H9MG) by developing an unbiased γ-secretase substrate identification (G-SECSI) method. We used the phase III clinical trial for semagacestat compound[38] and assayed the accumulation of substrate C-terminal fragments (CTFs). We identified 85 substrates, with 59 not known before to be cleaved by γ-secretases. Many of the identified substrates (e.g., CSF2RA, TNFRSF1B, TGFBR1, FCGR2A, and PILRA) are encoded by genes defining distinct microglial cell states.[39–41] We therefore used single-cell RNA sequencing to evaluate the cell states of the microglia in cell culture conditions, and *in vivo*, we used a microglia-specific γ-secretase conditional knockout (KO) mouse model. The results show that γ-secretases maintain a "low-level activated" basal state in the context of microglial cell culture and a HM basal state in microglia *in vivo*. Moreover, γ-secretase is crucial for the transition of HM to reactive cell states in the context of AD.

RESULTS

G-SECSI to identify substrates of γ-secretase

We developed the G-SECSI method to identify substrates in microglia (Figure 1A). H9MG (Figure S1) expresses the full spectrum of γ-secretase enzymes similar to primary human and mouse microglia (Figure S2). We prepared the membrane fractions (Step 2. Membrane protein purification under method details) that were fractionated on a Gel-eluted liquid fraction entrapment electrophoresis[42,43] system to separate FL proteins from their CTFs that accumulate when γ-secretase inhibitors are used. The different fragments of LRP1, a known substrate of γ-secretase, distributed nicely over the different fractions (Figure 1B). The LRP1 80-kDa fragment (generated by furin cleavage

Figure 1. γ-Secretase substrate identification using G-SECSI

(A) Schematic representation of G-SECSI procedure. Proteins are fractioned according to relative molecular weight (MW). MS on the different fractions allows for assigning identified peptides to either the C-terminal fragments (CTFs) or to the full-length (FL) protein.

(B) Western blot analysis of LRP1, a known γ-secretase substrate. Equal volume of each fraction was loaded, and the resulting blot was probed with the LRP1 C-terminal specific antibody (EPR3724). The lane at the left side displays the unfractionated lysate.

(C) Faceted bar plot showing the relative abundance of each detected peptide of LRP1 in the corresponding fraction as identified by MS analysis. On the right side, the position of the first aa of each specific peptide in LRP1-FL is indicated. The green horizontal line shows the start of the LRP1-CTF (*in silico* determination of carboxyterminal fragment under method details section). The blue double horizontal lines indicate the borders of the transmembrane domain (TMD) based on UniprotKB.[45] The green verticle line separates the fractions in which LRP1-CTF-derived peptides (left side) and LRP1 80-kDa fragment-derived peptides distribute. Q3 is quadrant 3 region defined by the horizontal and vertical green lines, where LRP1-CTF-derived peptides should be detected.

(D) Reference plot showing the mean and the 95% confidence interval of the protein size in each fraction. This plot is generated using MW and distribution of the fragments of known substrates detected in the different fractions.

(E) Faceted bar plot of γ-secretase substrate candidate SEMA4C. The faceted bar plots were derived from four independent experiments. Control (left) and semagacestat-treated (right) samples are indicated. The green horizontal line and blue double horizontal lines are as above. Q3 defines the area where SEMA4C-CTF-derived peptides should distribute.

of the 600-kDa protein)[44] distributes in fractions 10–12 and remains unchanged in treated and control conditions. In fractions 3–4 of the semagacestat-treated sample a clear accumulation of LRP1-CTF is seen, in contrast to the faint bands in the control condition. Thus, the fractionation method allowed us to separate efficiently the CTF that accumulates after γ-secretase inhibition from the FL protein.

We next analyzed each fraction by MS and obtained a visual representation of the peptide distribution over the different fractions in faceted bar plots, exemplified in Figure 1C. The plots show the relative abundance of all the tryptic peptides per fraction identified for a particular protein, ranked according to their position in the FL protein (Step 5. Spectral pattern visualization of target protein under method details section). These plots thus provide a semi-quantitative overview of all identified peptides and their localization in the protein. The peptides generated from the LRP1-CTF migrate in quadrant 3 (Q3), whereas the same peptides when generated from the LRP1-80-kDa protein migrate in Q4. Notice that the C-terminal peptides of LRP1 mainly detected in Q4 in the untreated condition accumulate after semagacestat treatment in Q3. These Q3 peptides are confirmed to be derived from the 14-kDa LRP1-CTF by γ-secretase cleavage (Figure 1B). Thus, by analyzing the tryptic peptides in each fraction and quantifying their distribution in Q3, we can assess whether a membrane-bound protein is a candidate γ-secretase substrate or not.

Identification of γ-secretase substrates in H9MG

We repeated four independent G-SECSI experiments using H9MG (Figure S3A). We loaded 600 μg membrane protein and collected 12 fractions per run. We identified and quantified 60,044 ± 5,417 (mean ± SD) peptides per experiment and assigned them to 6,009 ± 86 (mean ± SD) proteins, of which about 50% were membrane proteins (Figure S3B). Eventually, we extracted the single-pass type I and type III membrane protein subset covered by 4,285 ± 734 (mean ± SD) peptides assigned to 343 ± 10 (mean ± SD) specific proteins per experiment for further analysis.

Figure 1E shows the results obtained for the γ-secretase substrate candidate human semaphorin-4C (SEMA4C). *Sema4c* becomes upregulated in microglia after spinal cord injury and might play a role in microglial-mediated wound recovery.[46] The double blue horizontal lines indicate that the transmembrane domain (TMD) of SEMA4C is between amino acid (aa) 664 and aa 684. The single green horizontal line indicates the position of aa 604, which is the putative start of the CTF (*in silico* determination of carboxyterminal fragment under method details section). The predicted size of SEMA4C-FL (based on the number of aa) is 91.6 kDa and therefore should distribute in fractions 11–12, and the predicted SEMA4C-CTF of 25.3 kDa should distribute in fractions 3–6 (Figures 1D and 1E). The green vertical dotted line between fractions 6 and 7 separates the peptides in Q4 derived from SEMA4C-FL and the peptides in Q3 derived from SEMA4C-CTF. The peptides accumulate in Q3 when semagacestat is used, indicating that the SEMA4C-CTF in the control conditions is cleaved by γ-secretase.

We performed this analysis for the 359 detected specific single-pass type I and type III membrane proteins from H9MG. The faceted bar plots are accessible on our website https://data.

bdslab.org. We compared the relative abundance of the CTF-derived peptides in semagacestat vs. control conditions and identified in total 85 γ-secretase substrate candidates, of which 59 proteins (69%) were not known to be cleaved by γ-secretase (Table S1). The identified substrates are indicated in the volcano plot (Figure 2A, threshold: p.adj < 0.05 and fold change [FC] ≥ 1.2), and the relative abundance of their potential CTF-derived peptides across the four biological replicates are indicated in the heatmap (Figure 2B), which also demonstrates the high reproducibility of this method over the four independent experiments.

Validation of the identified γ-secretase substrate candidate

We selected three substrate candidates from the list, i.e., TNFRSF1B (FC = 1.66, p.adj = 0.0234), CD300A (FC = 1.67, p.adj = 0.0001), and MILR1 (FC = 1.32, p.adj = 0.0017), which are slightly above the threshold for assigning them as γ-secretase substrates (Figure 2A). We cloned the cDNA of these candidates and inserted a FLAG epitope into their C termini. We transfected the plasmids in HEK293T cells, treated the cells with semagacestat or DMSO for 16 h, and analyzed the cell lysates by western blot (Figure 2C). Probing the membrane with the FLAG antibody revealed a 29-kDa band from TNFRSF1B, a 20-kDa band from CD300A, and a 20-kDa band from MILR1, which accumulate upon semagacestat treatment. These results show that even the candidates that were identified at the lower threshold of the assay are reliable γ-secretase substrates.

γ-Secretase substrates are central in intracellular microglial signaling

Gene ontology (GO) analysis suggests that the identified γ-secretase substrates are involved in various microglial biological processes, including proliferation, phagocytosis, cytokines production, axon guidance, and migration (Table S2). "Transmembrane receptor protein kinase activity" (p.adj = 1.36E−09) and "cytokine binding" (p.adj = 1.36E−09) are the most significantly enriched molecular function GO terms (Table S2). Accordingly, six receptor tyrosine kinases (AXL, CSF1R, EPHA2, EPHB2, EPHB3, and MERTK) were identified (Table S1). Furthermore, four interleukin receptors (IL10RB, IL18R1, IL1RAP, and IL6ST), three tumor necrosis factor receptors (TNFRSF1A, TNFRSF1B, and TNFRSF21), and two colony-stimulating factor receptors (CSF1R and CSF2RA) are in the "cytokine-cytokine receptor interaction" pathway (Table S3). Interestingly, 53 out of 85 (62%) substrates are encoded by genes that are part of the transcriptional changes defining specific microglial states in AD models (Figure 3).[39,40,47] Half of these substrates (26/53) are encoded by HM genes. Sixteen substrates are encoded by typical "disease-associated microglia" or DAM genes (e.g., *GPNMB* and *GYPC*), human leukocyte antigen (HLA) microglial genes (e.g., *HLA-A* and *PILRA*) and "interferon response microglia" or IRM genes (e.g., *TLR2* and *CD163*). Proteins harboring the immunoreceptor tyrosine-based activation motif (ITAM: GPNMB, FCGR2A, and TYROBP) or the immunoreceptor tyrosine-based inhibitory motif (ITIM: CD300A, CD300LF, MILR1, LAIR1, and PILRA) are also identified as γ-secretase substrates (Table S1). ITAM- and ITIM-bearing receptors are known to play distinct roles in activating and inhibitory signaling transduction in microglia.[48,49] Hence, our findings suggest a role of γ-secretase
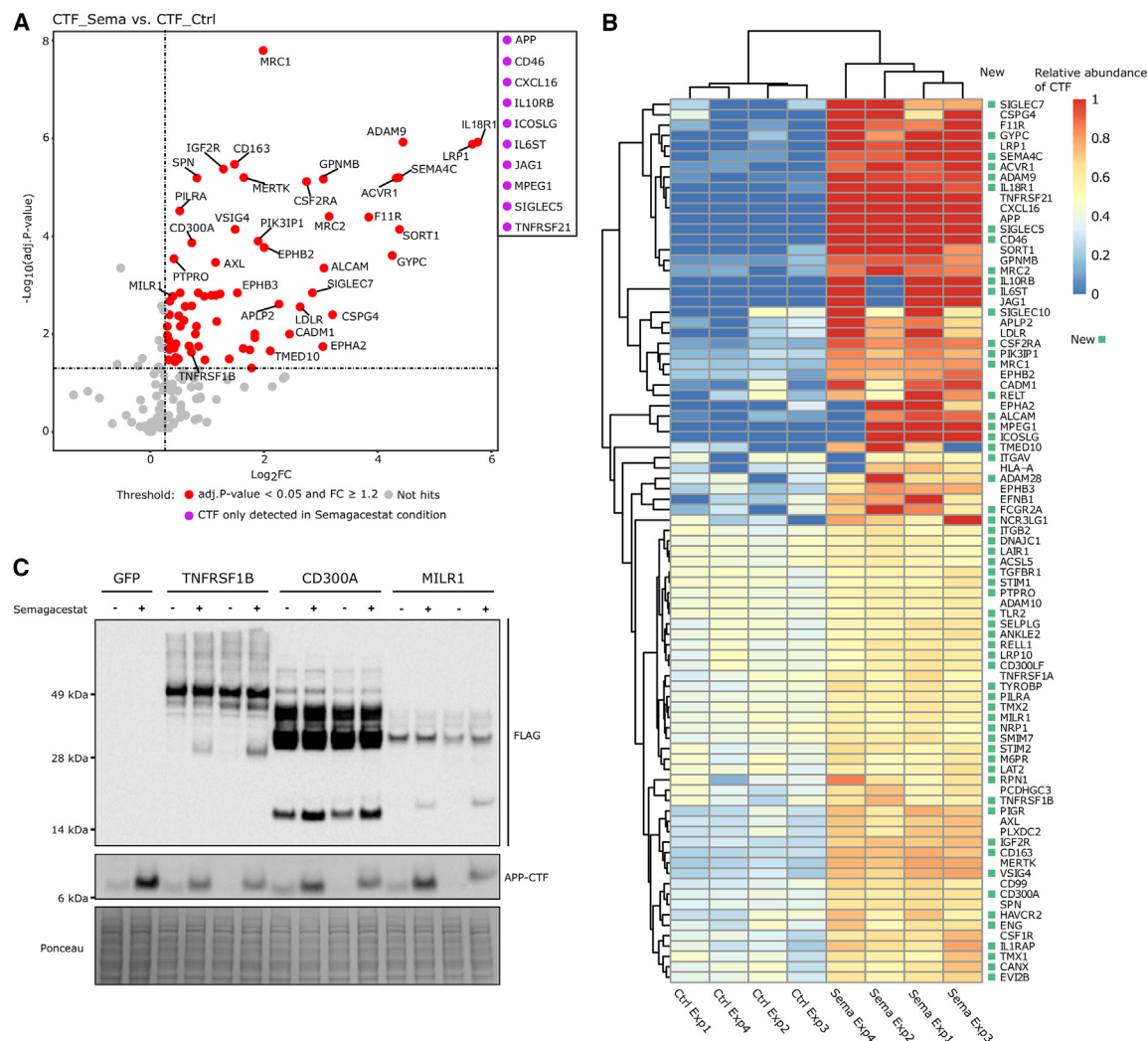
Figure 2. Overview of γ-secretase substrates in H9MG human microglia-like cells.

(A) Volcano plot showing the relative increase of CTF peptides in the presence of semagacestat vs. control. Proteins accumulating CTF only after treatment with semagacestat are indicated by purple dots in the insert at the top right. Every substrate has been confirmed in at least three out of four independent experiments and with fold change ≥ 1.2 and p.adj < 0.05, using Student's t test followed by Benjamini-Hochberg false discovery rate correction.

(B) Heatmap of the relative abundance of CTF proteins identified as γ-secretase substrates over four experiments. Substrate candidates that were not discussed before in the literature are indicated with green squares (left side of protein names).

(C) Validation of identified γ-secretase substrate candidates. TNFRSF1B, CD300A, and MILR1 cDNA tagged with FLAG were expressed in HEK293T cells, and extracts were analyzed by western blots using FLAG M2 mAb. Empty vector expressing GFP was used as negative and endogeneous APP-CTF accumulation as positive control. Ponceau staining is shown as loading control.

in maintaining a dynamic equilibrium between different cellular signals via cleaving distinct substrates in microglia. We reasoned that investigating the overall profile of the transcriptomes of the microglia would provide a good integrated readout for the overall context-dependent effect of blocking the processing of >85 γ-secretase substrates.

γ-Secretase inhibition causes substantial changes of microglial transcriptomes but does not affect the strong cell-state response to lipopolysaccharide (LPS) in vitro

We analyzed the single-cell transcriptomes of H9MG before and after semagacestat treatment under in vitro cell culture condi-

tions. We performed a second experiment in parallel, treating cell cultures with LPS, asking whether a strong γ-secretase-independent signal could overcome the transcriptional changes induced by semagacestat. The LPS response is largely mediated by the specific receptor TLR4,[50] which is not cleaved by γ-secretase (Figure S4).

We obtained a total of 17,006 single transcriptomes across the 4 different conditions: normal cell culture (Ctrl), semagacestat treated (Sema), LPS treated (LPS), and semagacestat/LPS treated (SemaLPS) (Figures 4A, 4B, and S5). As expected, LPS treatment induced a strong response[51] (Figure 4B). Semagacestat treatment did not alter LPS-induced gene expression
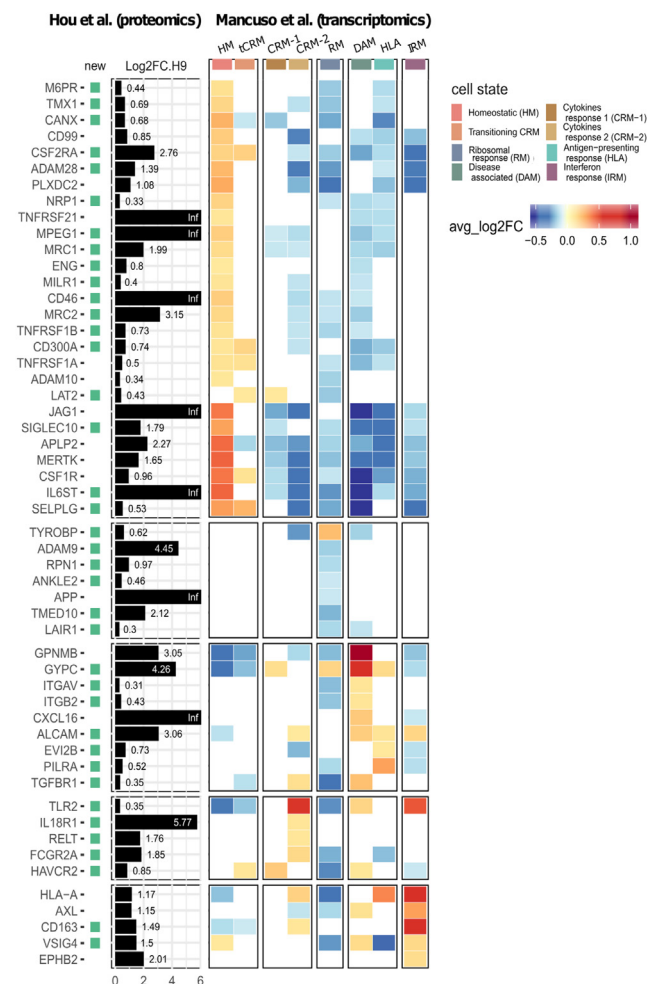
Figure 3. γ-Secretase substrates are highly involved in microglial cell-state regulation

Combined plots showing substrates encoded by human microglial cell-state-defining genes organized per cell state as defined by Mancuso et al.[39] Cell-state-defining genes are the most significantly upregulated or downregulated genes in a particular microglial cell state vs. cells in the other states. |avg_log2FC| > 0.1 using Bonferroni correction (p.adj < 0.05). The black bars represent the log2FC of the CTF relative abundance of the substrates in semagacestat condition vs. control condition. The heatmap summarizes the differential expression (log2FC, color scale) of the corresponding genes in the particular cell states (each cluster compared with all others). HM, homeostatic; (t)CRM, (transitioning) cytokine response; RM, ribosomal; DAM, disease associated; HLA, HLA response; IRM, interferon response.

(Figure 4C). Thus, LPS drives the cell state independently of γ-secretase activity.

We separated the 8,611 and 8,395 single H9MG transcriptomes in the normal and the LPS-stimulated conditions, respectively, and analyzed those individually. Using unbiased clustering, we identified cell clusters CC1, CC2, and CC3 in the normal culture condition (Figure 4D) and LPS1, LPS2, and LPS3 in the LPS-stimulated condition (Figure 4I). Semagacestat treatment mildly shifted the distribution of cells between clusters CC1 and CC2 (Figures 4E and 4F) and between clusters LPS1 and LPS2 (Figures 4J and 4K). We analyzed the top expressed genes in these clusters

(Figures S6A, S6B, S6D, and S6E). Cells in clusters CC2 and LPS2 expressed higher typical HM genes (such as *C1QA*, *MAF*, and *NAIP*) and HLA genes (such as *MS4A6A*, *HLA-DMB*, and *HLA-DRB1*), compared with their counterparts CC1 and LPS1 expressing higher typical DAM genes (such as *CD9*, *SPP1*, and *ORL1*). Trajectory analysis with Monocle 3, aligning cells along the trajectories from CC2 to CC1 and from LPS2 to LPS1, confirmed rather mild effects on cell states caused by semagacestat treatment (Figures 4G and 4L).

The impact of semagacestat treatment on gene expression however becomes evident in gene differential expression (DE) and gene set enrichment (GSEA) analyses. These analyses demonstrate that 350 genes are significantly (p.adj < 0.05) upregulated or downregulated in Sema cells, compared with control cells (Figures 4H and S6C), whereas 267 genes are significantly upregulated or downregulated in the SemaLPS vs. LPS conditions (Figures 4M and S6F). Notably, in both control and LPS conditions, semagacestat induces upregulation of HM genes (e.g., *C1QA*, *MAF*, *NAIP*, etc.) and downregulation of DAM genes (e.g., *CD9*, *SPP1*, *OLR1*, etc.)[39,40] (Figures S6C and S6F). Thus, γ-secretase seemingly regulates the expression levels of a similar set of genes in control and under LPS stress.

γ-Secretase deficiency alters cell signaling in microglia *in vivo*

We crossed the *Cx3cr1*[CreERT2/WT] mice[52] with the *Aph1a*^{fl/fl}*b*[−/−]*c*[fl/fl] mice[53] to generate the microglia-specific γ-secretase conditional KO mice (*GS*[iΔMG], Figure 5A). We induced the KO at 1 month of age by treating the mice for 5 consecutive days with tamoxifen. We analyzed the single-cell transcriptomes of 7,285 microglia from 3-month-old mice and obtained 4 microglia clusters (Figures 5B and 5C). While a very small cluster 3 marked by the relatively high expression of DAM genes was significantly enriched with *GS*[iΔMG] microglia (Figures 5D and 5E), the overall effect of γ-secretase deficiency on cell states is limited as it was in the cell culture experiments.

In contrast, DE and GSEA analyses revealed that 919 genes were significantly differentially regulated (p.adj < 0.05, abs(avg_Log2FC) > 0.1) by γ-secretase deficiency. Those genes that were upregulated had a stronger DAM profile, while those that were downregulated were more HM (Figures 5F–5H). DE analysis between *GS*[iΔMG] and *GS*[WT] microglia on a per-cluster basis showed that representative DAM genes (e.g., *Ctsl*, *Cd9*, *Timp2*, *H2-D1*, *Ctsb*, and *Lyz2*) were consistently upregulated in the *GS*[iΔMG] condition across all clusters (Figure 5I). This suggests that disrupting γ-secretase modulates the global gene expression of a cluster of genes associated with microglial activation,[37,47,54] without changing overall cell states as determined by the Louvain clustering algorithm.

γ-Secretase deficiency impedes the formation of activated microglial cell states in *App*[NL-G-F] mice

Given the preponderance of the γ-secretase substrates involved in AD-related microglial cell states (Figure 3) and the altered HM and DAM genes expression in the *in vitro* (Figure 4) and *in vivo* (Figure 5) experiments, we decided to investigate the effects of γ-secretase deficiency on microglia exposed to amyloid plaques. We further crossed the *GS*[iΔMG] mice with the *App*[NL-G-F] model for
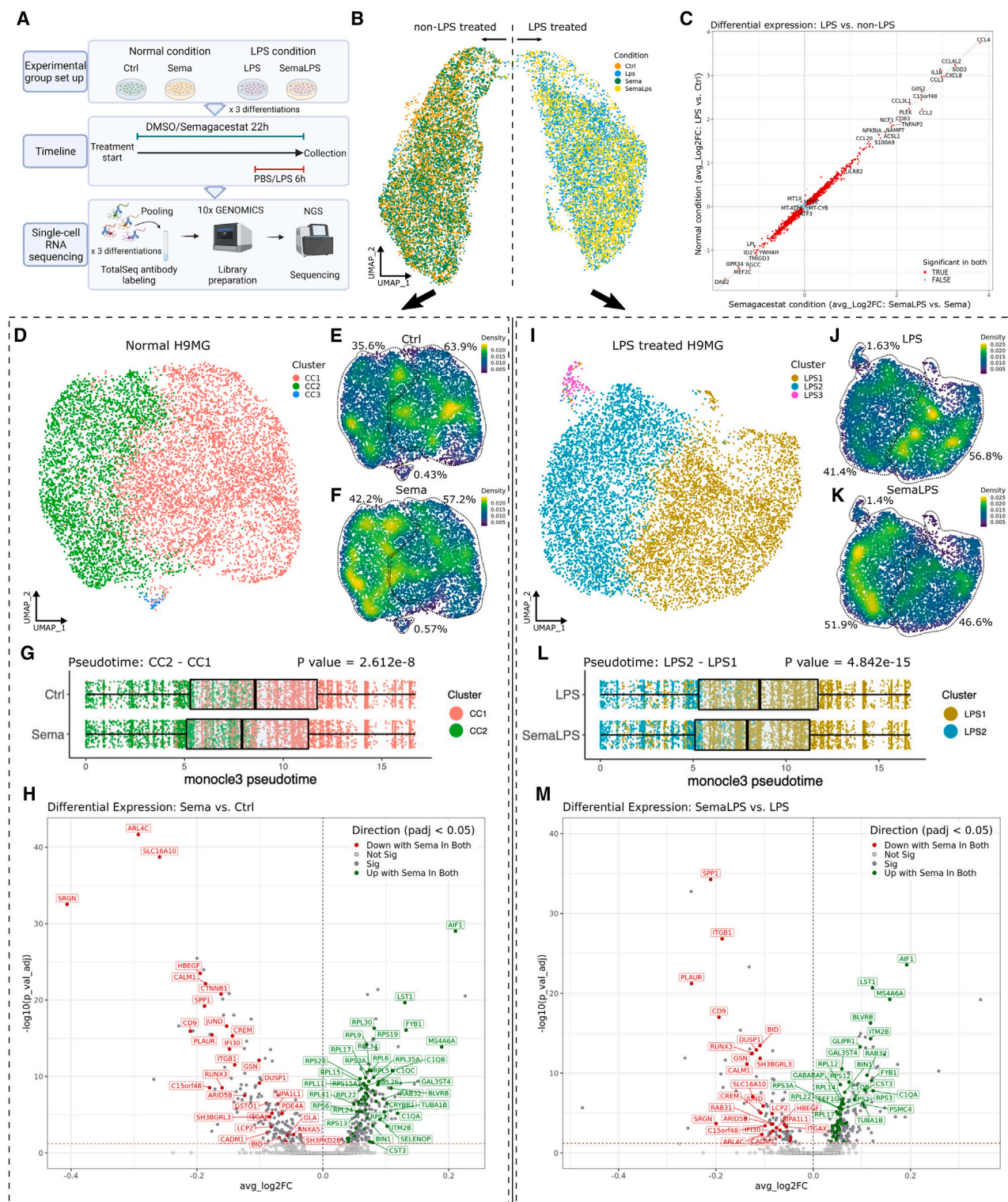
Figure 4. γ-Secretase inhibition alters microglial steady-state signaling *in vitro*

(A) H9MG cells were collected for single-cell RNA sequencing from four conditions: Ctrl (vehicle), Sema (semagacestat), LPS (vehicle treatment for 22 h with last 6 h exposure to LPS), and SemaLPS (semagacestat treatment for 22 h with last 6 h exposure to LPS). n = 3 independent differentiations per condition.

(B) Uniform manifold approximation and projection (UMAP) showing 17,006 single H9MG passing quality control after removal of the proliferative subpopulation. Cells are colored according to the four different conditions.

(legend continued on next page)

AD[55] to generate the App^{NL-G-F}-$GS^{i\Delta MG}$ mice. We reasoned that the transcriptomic alterations we recorded previously in healthy conditions might be more easily picked up as cell-state transitions in a disease model.[37,47,54] The tamoxifen-induced KO mice (App^{NL-G-F}-$GS^{i\Delta MG}$), the vehicle-treated control mice (App^{NL-G-F}-GS^{WT}), as well as the mice for tamoxifen-induced artifact controls (App^{NL-G-F}-TAM_QC and App^{NL-G-F}-Ctrl_QC) are indicated in Figure 6A. We induced the KO at 1 month of age with tamoxifen and analyzed the single-cell transcriptomes of 37,884 microglia (Figure S7) from 3-month-old mice and from 6- to 7-month-old mice, which showed mild and advanced amyloid pathology, respectively. Unbiased clustering using Seurat resulted in six main clusters (Figures 6B and 6C), named homeostatic (HM), cytokine response (CRM), transitioning cytokine response (tCRM), interferon response (IRM), transition response (TRM), and disease-associated microglia (DAM), referring to previous work[37,39,41,47,54] (Figures S8A–S8C). A small "pre-DAM" cluster whose partially overlapping HM and DAM signature represents an intermediate cell state (Figures 6B and 6C) is of particular interest, because it is only seen in the App^{NL-G-F}-$GS^{i\Delta MG}$ mice (Figure S8D). Moreover, pre-DAM cells highly express the subset of DAM genes (e.g., *Ctsl*, *Cd9*, *Timp2*, *Ctsb*, and *Lyz2*) that represents the disrupted microglial signaling shown in the $GS^{i\Delta MG}$ mice in Figure 5, whereas the expression levels of other known DAM signature genes (e.g., *B2M*, *Axl*, *Cst7*, *Lpl*, and *Lilrb4a*) are not as pronounced (Figure S8E).

We compared the single microglial transcriptomes in the six indicated conditions (n = 4 animals per condition). The shifts in microglial distribution across different cell states caused by γ-secretase deficiency were mild at 3 months but obvious at 7 months (Figures 6D and 6E). The relative proportions of DAM, CRM, and TRM were significantly reduced in App^{NL-G-F}-$GS^{i\Delta MG}$ mice, compared with App^{NL-G-F}-GS^{WT} mice, at 7 months, whereas HM and tCRM were significantly increased (Figure 6G). Interestingly, the pre-DAM cluster was significantly enriched in both 3- and 7-month-old App^{NL-G-F}-$GS^{i\Delta MG}$ mice, compared with their age-matched App^{NL-G-F}-GS^{WT} mice (Figure 6G). DE analysis between microglia of App^{NL-G-F}-$GS^{i\Delta MG}$ mice and microglia of App^{NL-G-F}-GS^{WT} mice at 7 months echoed that the reduced proportion of the DAM cluster revealed the upregulation of HM genes and the downregulation of DAM genes (Figure 6I). A DE analysis of microglial transcriptomes between the two γ-secretase conditions on a per-cluster basis confirmed that the same group of genes (e.g., *Ctsl*, *Cd9*, *Timp2*, *Ctsb*, and *Lyz2*) was consistently upregulated in the App^{NL-G-F}-$GS^{i\Delta MG}$ groups at both 3 and 7 months across the main clusters (Figures 6K and 6L). Thus, disrupting γ-secretase has a general effect on all the γ-secretase-deficient microglia, as in the cell cultures and the control mice, next to its blocking effect on cell-state transitions driven by the amyloid plaques.

Tamoxifen treatment alone, comparing App^{NL-G-F}-TAM_QC and App^{NL-G-F}-Ctrl_QC samples, showed only mild effects, with a small decrease in the DAM cluster but no effects in other clusters (Figures 6F and 6G). DE analysis also confirmed that the tamoxifen-induced artifact was limited (Figure 6J) and did not affect the expression of genes regulated by γ-secretase (e.g., *Ctsl*, *Cd9*, *Timp2*, *Ctsb*, and *Lyz2*; Figure 6M).

To exclude the potential effect of the genetic modification (floxed *Aph1a/c* alleles and *Aph1b* KO)[53] on microglial cell states in the AD context, we compared the tamoxifen-untreated App^{NL-G-F} × *Aph1Floxed* mice (App^{NL-G-F}-GS^{WT}) and the App^{NL-G-F} mice at 12 months of age. We analyzed 5,999 single microglial transcriptomes from the App^{NL-G-F} x *Aph1Floxed* mice and 7,185 transcriptomes from the App^{NL-G-F} mice. All the typical microglial transcriptomic cell states (HM, DAM, CRM, IRM, and TRM) as previously described[47] were identified and annotated in the uniform manifold approximation and projection (UMAP) (Figures S9A–S9C). The genetic modification in the App^{NL-G-F} × *Aph1Floxed* mice did not significantly change the distribution of microglia across the different cell states, compared with the age-matched App^{NL-G-F} mice (Figures S9A–S9D). This confirms that the alterations observed in the experiments above can be attributed to γ-secretase deficiency induced by tamoxifen treatment and not to the genetic construct as such.

Taken together, the results indicate that γ-secretase deficiency alters the expression of a series of specific genes in microglia in different cell environments and majorly impedes the formation of *in vivo* activated microglial cell states induced by amyloid plaque exposure (DAM, TRM, and CRM), as evidenced in 7- vs. 3-month-old animals.

γ-Secretase deficiency blocks *in vivo* microglia in a pre-DAM state in response to amyloid pathology

Using Monocle 3 and assuming a transition from the HM to other cell states (Figure 7A), two major pseudotime trajectories from

---

(C) Quadrant plot showing the similarity of the LPS response in the vehicle (y axis) and in the semagacestat condition (x axis). Wilcoxon rank-sum test, p values adjusted with Bonferroni correction (p.adj < 0.05).

(D–F) UMAPs showing 8,611 single H9MG transcriptomes from Ctrl and Sema-treated conditions retrieved from (B). Two main clusters (CC1 and CC2) and a small cluster (CC3) are identified (D). Density plots showing the distribution of H9MG cells across the three clusters in Ctrl (E) and Sema (F) conditions.

(G) Plots showing the delayed phenotypic trajectory of H9MG cells caused by γ-secretase inhibition (pseudotime ordering with Monocle 3 and colored by the cell states shown in D).

(H) Volcano plot showing the gene differential expression in non-proliferative H9MG cells in Sema vs. Ctrl. Wilcoxon rank-sum test, p values adjusted with Bonferroni correction (p.adj < 0.05). The genes upregulated and downregulated by semagacestat in both the non-LPS condition (H) and the LPS condition (M) are colored in green and red, respectively.

(I–K) UMAPs showing 8,395 single H9MG transcriptomes from LPS and SemaLPS conditions retrieved from (B). Two main clusters (LPS1 and LPS2) and a small cluster (LPS3) are identified (I). Density plots showing the distribution of H9MG cells across the three clusters in LPS (J) and SemaLPS (K) conditions.

(L) Plots showing delayed phenotypic trajectory of H9MG cells caused by γ-secretase inhibition (pseudotime ordering with Monocle 3 and colored by the cell states shown in I).

(M) Volcano plot showing the gene differential expression in SemaLPS vs. LPS. Wilcoxon rank-sum test, p values adjusted with Bonferroni correction (p.adj < 0.05). The genes upregulated and downregulated by semagacestat in both the non-LPS condition (H) and the LPS condition (M) are colored in green and red, respectively.

Figure 5. γ-Secretase deficiency alters microglial signaling *in vivo*

(A) Mice were treated with tamoxifen or vehicle at 1 month of age and sacrificed at 3 months.

(B and C) UMAP showing 4,376 single mouse microglia from 4 GS^{WT} mice (B) and 2,909 single mouse microglia from 3 $GS^{i\Delta MG}$ mice (C).

(D) Top 10 differentially expressed genes per cluster. The size of each dot represents the percentage of cells expressing the indicated gene within the cluster, and the color represents the scaled and normalized average expression of the indicated gene.

(E) Boxplots showing proportion of cells across the clusters. Multiple unpaired Student's t test corrected by Bonferroni method. n = 3–4 biological replicates per condition. *p < 0.05; ns, not significant.

(F) Volcano plots showing the gene differential expression in mouse microglia of $GS^{i\Delta MG}$ vs. GS^{WT}. Wilcoxon rank-sum test, p values adjusted with Bonferroni correction (p.adj < 0.05).

(legend continued on next page)

HM toward DAM and CRM emerge (Figures 7B and 7C). These align with previously reported human microglial responses in a chimeric AD model.[39] A third trajectory toward IRM (gray dotted line) was not further considered, as the IRM cell state was not affected by γ-secretase deficiency (Figure 6G). Particularly at 7 months, microglial distributions along the HM-tCRM-CRM and the HM-TRM-DAM axes are shifted toward higher pseudo-time values in $App^{NL-G-F}-GS^{WT}$ mice, while in $App^{NL-G-F}-GS^{i\Delta MG}$ mice, they reside mostly in HM, tCRM, and pre-DAM states (Figures 7D–7F). Regression analysis comparing the transcriptomic profiles of microglia in 7- vs. 3-month-old brains in the deficient or control γ-secretase condition (Figure 7G) confirms a significantly attenuated age-dependent microglial activation in the $App^{NL-G-F}-GS^{i\Delta MG}$ mice. Of note, age here reflects increased amyloid plaque accumulation.

TREM2 is cleaved by γ-secretase,[32] important for TREM2 downstream signaling.[56] TREM2 KO blocks microglia in a so-called DAM1 state in *TgAD* mice.[37] DAM1 expresses only a subset of the DAM program and lacks the Trem2-dependent lipid metabolism (*Lpl* and *Ccl6*) and phagocytic pathway genes (*Axl*, *Clec7a*, and *Ctsl*) characteristic of a full DAM response.[37] pre-DAM microglia accumulate when DAM is abolished in $App^{NL-G-F}-GS^{i\Delta MG}$ mice, leading us to wonder if pre-DAM is a DAM1-like state. Interestingly, while the low expression of *Axl*, *Cst7*, *Lpl*, and *Lilrb4a* in pre-DAM aligns with what has been described in DAM1, the high expression of *Cd9*, *Ctsl*, *Spp1*, and *Timp2* in pre-DAM conflicts with the reported DAM1 features (Figure S8E). We next performed a Pearson's correlation analysis between the FCs of genes in pre-DAM vs. DAM identified in this study and DAM1 vs. DAM2 identified previously by Keren-Shaul et al. but find only a weak correlation (Figure S8F, R = 0.35). Therefore, the perturbation of microglial states caused by γ-secretase deficiency is distinct from that previously reported in the *Trem2* KO condition.[37]

We finally compared morphological microglial phenotypes and amyloid pathologies in 7-month-old $App^{NL-G-F}-GS^{i\Delta MG}$ and $App^{NL-G-F}-GS^{WT}$ mice using immunofluorescent staining. The total area covered by microglia (EYFP+) is similar between the two genotypes (Figures 7H and 7I). However, while the γ-secretase potent microglia formed large clusters around the plaques, γ-secretase-deficient microglia remained nicely distributed in a tilted fashion in the presence of amyloid plaques (Figures 7H, 7J, and 7K). There was no clear difference in amyloid plaque load (Figure 7L). Taken together, consistent with the single-cell transcriptomic analysis, γ-secretase deficiency blocks microglial response to Aβ plaques.

DISCUSSION

Using the G-SECSI method to survey the membrane proteomes of H9MG cells in the presence or absence of the γ-secretase inhibitor semagacestat, we identify a remarkable large number of substrates (85) processed by γ-secretase in steady-state cell culture conditions. The only precedent study that tried to unbiasedly identify substrates by separating the CTF and FL proteins using conventional SDS-PAGE yielded 13 γ-secretase substrates in HeLa cells.[22] Our method seems more precise and sensitive and brings home the message that even under normal cell culture conditions, γ-secretase cleaves many substrates in parallel. Most are important signaling molecules, including tyrosine receptor kinases (AXL, CSF1R, EPHA2, EPHB2, EPHB3, and MERTK), interleukin receptors (IL10RB, IL18R1, IL1RAP, and IL6ST), tumor necrosis factor receptors (TNFRSF1A, TNFRSF1B, and TNFRSF21), ITAM receptors (GPNMB, FCGR2A, and TYROBP), ITIM receptors (CD300A, CD300IF, MILR1, LAIR1, and PILRA), and so on (see Tables S1, S2, and S3). γ-Secretase activity thus appears in the center of a variety of crucial signaling pathways in microglia.

It is unexpected that so many substrates are processed by γ-secretase in parallel under, assumed, steady-state conditions in cell culture. Indeed, γ-secretase cleavage is a highly regulated activity. Only a few substrates with natural short ectodomains can be cleaved directly,[57–59] while most need an activation step by another type of membrane-anchored protease, for instance, members of the "a disintegrin and metalloprotease" (ADAM) family.[60] This cleavage, which is also regulated, shortens the ectodomain of the candidate substrates so that they can be accommodated in the γ-secretase complex.[21] In addition, other proteins and lipids, for instance, tetraspanin-enriched microdomains, regulate γ-secretase activity.[61] A more recent study demonstrated that interferon-induced transmembrane protein 3 (IFITM3) activates γ-secretase in the presence of inflammatory cytokines, which positively regulate Aβ generation.[62] Therefore, we hypothesize that γ-secretase serves as the converging point of many different upstream regulatory events, while the available γ-secretase substrate proteome reflects a series of cues present in the cell culture.

We analyzed the transcriptome of *in vitro* microglia in the presence and absence of the γ-secretase inhibitor semagacestat to see how the inhibition of the processing of these proteins affects gene expression. The expression of 350 genes was altered (Figure 4H). We propose to extend the concept of "tonic signaling" to describe this effect on the expression of multiple genes in the absence of specific stimuli. The concept of tonic signaling was originally proposed in the field of lymphocyte biology and has been used to indicate the low-level constitutive signaling in resting B lymphocytes and T lymphocytes as a result of a dynamic equilibrium between positive and negative signals.[63–65]

We were surprised that the alteration in tonic signaling caused by γ-secretase inhibition did not initiate a dramatic shift in cell states, i.e., that the cells with γ-secretase deficiency do not cluster drastically differently in the UMAP plots (Figures 4E, 4F, 4J, and 4K). Nevertheless, the tonic signaling defined as the change in gene expression brought on by blockage of γ-secretase is robust and remains discernible even in the background of a strong LPS-induced response (Figures 4H and 4M). Like the *in vitro* observations, genetic KO of γ-secretase induced mild

---

(G and H) Gene set enrichment analysis (GSEA) enrichment score curves. GSEA for the gene differential expression in mouse microglia of $GS^{i\Delta MG}$ vs. GS^{WT} was performed using HM and DAM gene sets[37,47] as reference. The DAM gene set is significantly enriched in genes that are upregulated (G), and the HM gene set is significantly enriched in genes that are downregulated (H) in γ-secretase-deficient cells.

(I) Heatmap showing the relative expression of the representative genes (identified in F) in $GS^{i\Delta MG}$ vs. GS^{WT} across all the identified clusters.
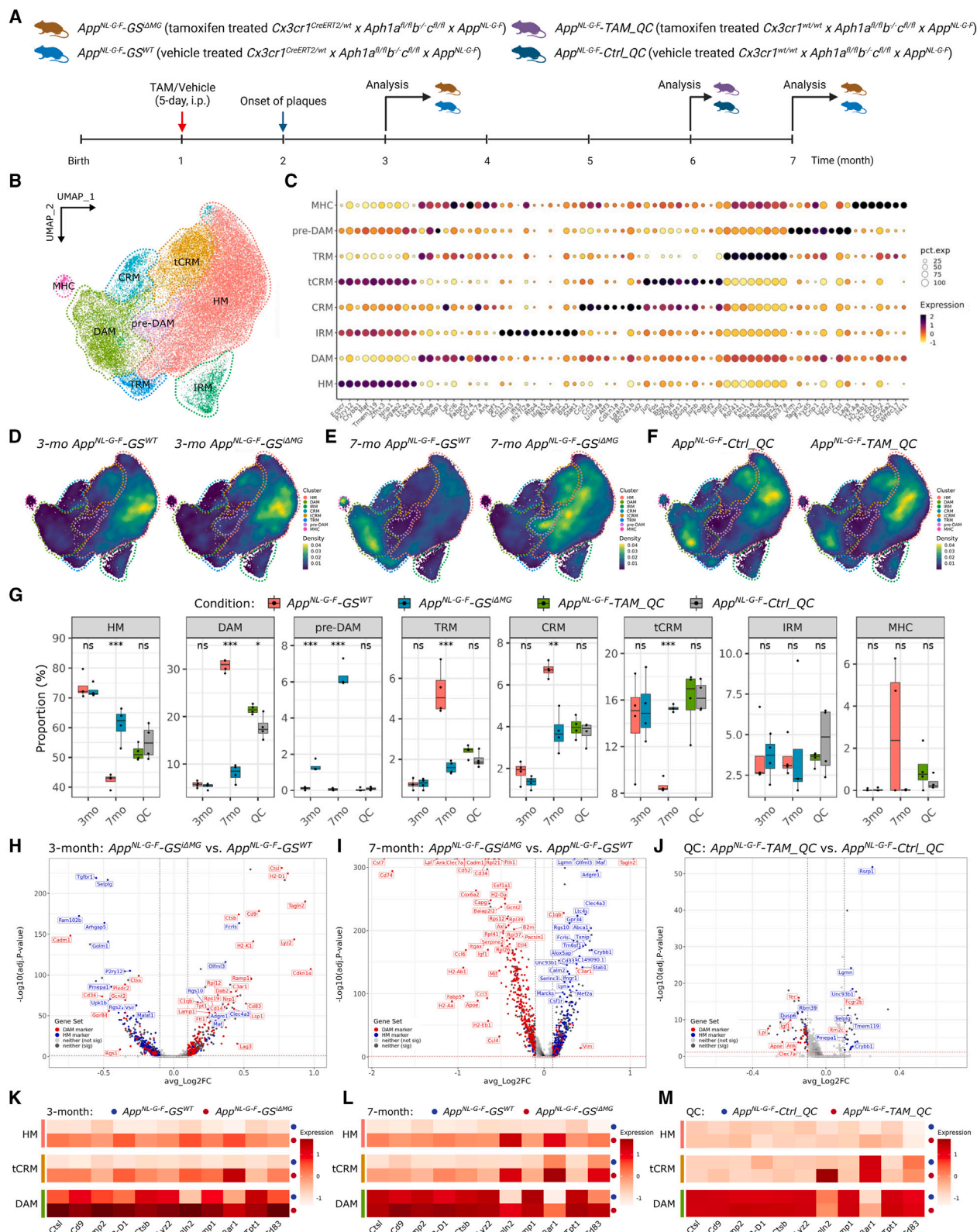
(legend on next page)

changes to the transcriptomic cell states of microglia in control mice (Figure 5). Nevertheless, we observed that γ-secretase inactivation affected differential gene expression of >900 genes, confirming that the enzyme broadly regulates gene expression in a tonic way. The observed lack of shift in cell states is somewhat puzzling. One possible explanation is that the differential gene expression induced by γ-secretase inhibition, despite encompassing hundreds of genes, may be not strong enough to drive affected cells into separate clusters. In agreement with this interpretation, the microglia showed a consistent upregulation of a group of genes (e.g., *Ctsl*, *Cd9*, *Timp2*, *Ctsb*, and *Lyz2*) independent of their assigned cell states (Figure 5I). Interestingly, these genes are a subset of previously described DAM signatures.[37,47] Thus, our results suggest that normal γ-secretase activity promotes activating gene expression *in vitro* and HM gene expression *in vivo*—the natural states of microglia in these two conditions.[66,67] We suggest that the main function of γ-secretase is the integration of a diverse array of extracellular signals provided by the cell's environment, resulting in a basal signaling state onto which additional signals (via γ-secretase or other signaling mechanism) can be superimposed.

The altered expression of HM and DAM genes induced by γ-secretase deficiency in the *in vitro* (Figure 4) and *in vivo* (Figure 5) experiments made us wondering whether γ-secretase was involved in the regulation of microglial responses to amyloid pathology in AD. We therefore generated a specific microglial γ-secretase KO in the App^{NL-G-F} mouse model. This experiment, in line with what we concluded above, demonstrated that γ-secretase deficiency mildly altered the microglial states in 3-month-old App^{NL-G-F}-$GS^{iΔMG}$ mice, when amyloid pathology is mild, all the while inducing the same gene set that reflects dysregulated tonic signaling by γ-secretase as seen in the wild-type condition (*Ctsl*, *Cd9*, *Timp2*, *Ctsb*, *Lyz2*, etc.). At 7 months however, the DAM response in App^{NL-G-F}-$GS^{iΔMG}$ mice was severely attenuated, compared with the control situation. Accordingly, γ-secretase-deficient microglia showed abnormal phenotypic responses to the Aβ plaques in the brains of App^{NL-G-F}-$GS^{iΔMG}$ mice (Figure 7H). Thus, γ-secretase has a crucial role in the microglial transition from the HM to the full DAM phenotype in AD. Apparently, in the context of the amyloid pathology, this effect is strong

enough to affect the clustering of single cells into cell states. Using transcriptomic analyses, we show that this blockage induced by γ-secretase deficiency is not equivalent to the blockage previously observed in $Trem2^{-/-}$ TgAD mice reported by Keren-Shaul et al.[37] So, while it is likely that the blockage of γ-secretase cleavage on Trem2 contributes to the overall disturbance in the microglia, it is clear that other substrates also play a role in this phenomenon. The DAM phenotype is considered by some as a protective mechanism in AD.[68,69] Thus, indiscriminate inhibition of γ-secretase to lower Aβ production in AD will not only cause Notch signaling disturbances[4] but is also predicted to cause microglial dysfunction as demonstrated in this study. These may ultimately have contributed to the failure of the semagacestat phase III clinical trial in 2013.[38,70]

Taken together, we investigate here in a systemic way the microglia-specific γ-secretase substrate proteome and provide evidence that γ-secretase regulates what we propose to call tonic signaling in microglia. The subset of proteins cleaved by γ-secretase activity at any moment reflects the cell state (which genes are expressed) and the cell environment (in this study: *in vitro* culture conditions or *in vivo* brain environment). This view substantially modifies the hypothesis that γ-secretase is merely responsible for clearing membranes from TMDs of proteins (as proposed by the "proteasome of the membrane" hypothesis)[8] and puts γ-secretase, at least in parallel to its degradation role, firmly as a central integrator of external cues into a consistent intracellular cell signal.

Limitations of the study

An important part of the γ-secretase cleavage occurring at any moment in time is regulated by the alpha, beta, and potentially other proteolytic activities that process the ectodomains of the substrates.[71] These ectodomain-shedding proteases contribute to the available protein substrate spectrum for γ-secretase processing, depending on biological conditions or cell types, and are an important part of the RIP cascade. This aspect was not investigated here. Although our study provides a powerful tool and a conceptual framework to investigate the role of γ-secretase herein, further studies are required to investigate the downstream signaling functions and how dysfunction in different cell

---

Figure 6. γ-Secretase deficiency perturbs microglial cell states in AD mouse brains

(A) Mouse microglia for single-cell RNA sequencing were isolated from mice with two genotypes ($Cx3cr1^{CreERT2/WT}$ × $Aph1a^{fl/fl}b^{-/-}c^{fl/fl}$ × App^{NL-G-F} and $Cx3cr1^{WT/WT}$ × $Aph1a^{fl/fl}b^{-/-}c^{fl/fl}$ × App^{NL-G-F}). Mice were treated with tamoxifen or vehicle at 1 month of age before Aβ plaques are formed and were sacrificed at one of the three indicated time points (3, 6, and 7 months).

(B) UMAP of the 37,884 single mouse microglia from 24 mice (6 conditions × 4 biological replicates per condition) passing quality control and after removal of non-microglial subpopulations. Eight clusters are indicated: homeostatic microglia (HM), cytokine response microglia (CRM), transitioning cytokine response (tCRM), interferon response microglia (IRM), disease-associated microglia (DAM/ARM), immature DAM (pre-DAM), transitioning response microglia (TRM), and antigen-presenting response microglia (MHC). Annotation is based on previous studies[39,41,47] (see Figures S8A–S8C).

(C) Top 10 differentially expressed genes in each identified cluster.

(D–F) Density plots showing the distribution of mouse microglia across the eight clusters in App^{NL-G-F}-GS^{WT} and App^{NL-G-F}-$GS^{iΔMG}$ mice at 3 months (D) and 7 months (E), and App^{NL-G-F}-Ctrl_QC and App^{NL-G-F}-TAM_QC at 6 months (F).

(G) Boxplots showing proportion of cells across all clusters in the different conditions, two-way ANOVA followed by Tukey's multiple comparison test. n = 4 biological replicates per condition. *p < 0.05; **p < 0.01; ***p < 0.001; ns, not significant.

(H–J) Volcano plots showing the gene differential expression in mouse microglia of App^{NL-G-F}-$GS^{iΔMG}$ vs. App^{NL-G-F}-GS^{WT} at 3 months (H) and 7 months (I), and also App^{NL-G-F}-TAM_QC vs. App^{NL-G-F}-Ctrl_QC at 6 months (J). Wilcoxon rank-sum test, p values adjusted with Bonferroni correction (p.adj < 0.05). The genes above the threshold and belonging to the previously described DAM/ARM and HM[37,47] are colored in red and blue, respectively.

(K–M) Heatmaps showing the relative expression of the representative genes (identified in $GS^{iΔMG}$, Figure 5I) across the main clusters in mouse microglia of App^{NL-G-F}-$GS^{iΔMG}$ vs. App^{NL-G-F}-GS^{WT} at 3 months (K) and 7 months (L), and also App^{NL-G-F}-TAM_QC vs. App^{NL-G-F}-Ctrl_QC at 6 months (M).
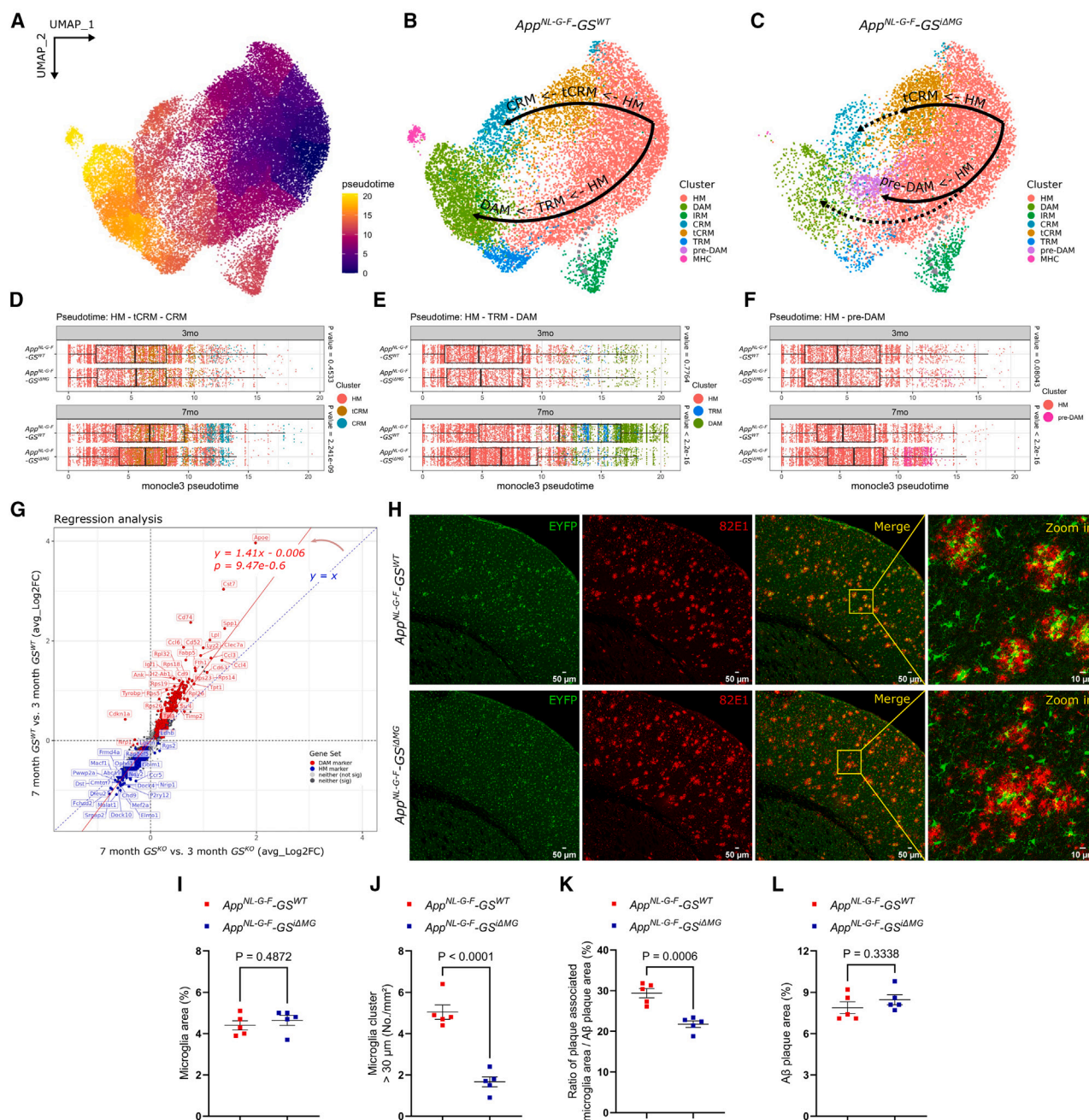
Figure 7. γ-Secretase deficiency blocks microglia in a pre-DAM state in response to amyloid pathology

(A) UMAP showing the phenotypic trajectory of *in vivo* microglia in response to amyloid pathology obtained by an unbiased pseudotime ordering with Monocle 3.

(B and C) UMAPs showing 13,694 single mouse microglia from 3- and 7-month *App^{NL-G-F}-GS^{WT}* mice (B), and 11,835 single mouse microglia from 3- and 7-month *App^{NL-G-F}-GS^{iΔMG}* mice (C). Arrows indicate the potential microglial activation routes determined by pseudotime analysis in (D)–(F), based on Mancuso et al.[39]

(D–F) Distribution of cells from *App^{NL-G-F}-GS^{WT}* and *App^{NL-G-F}-GS^{iΔMG}* mice along the three indicated transcriptional trajectories: HM – tCRM – CRM (D), HM – TRM – DAM (E), and HM – pre-DAM (F), colored by clusters (shown in B and C).

(G) Quadrant plot showing age-dependent microglial gene differential expression in *App^{NL-G-F}-GS^{WT}* mice (y axis) and in *App^{NL-G-F}-GS^{iΔMG}* mice (x axis). Linear regression analysis was performed on the log2FC of differentially expressed genes in the *App^{NL-G-F}-GS^{WT}* mice 7- vs. 3-month and the *App^{NL-G-F}-GS^{iΔMG}* mice 7- vs. 3-month comparisons (lm(*App^{NL-G-F}-GS^{WT}* 7 vs. 3 months ~ *App^{NL-G-F}-GS^{iΔMG}* 7 vs. 3 months)). To determine if the obtained slope was different from y = x, the t statistic was calculated by taking the absolute value of 1 (the slope of y = x) minus the calculated slope and dividing it by the standard error. The p value was obtained from this test statistic.

(H) Representative images of immunofluorescent staining of brain sections from 7-month *App^{NL-G-F}-GS^{WT}* and *App^{NL-G-F}-GS^{iΔMG}* mice. EYFP: microglia (green); 82E1: Aβ plaques (red).

types affects disease conditions. For our *in vitro* experiments, we have used microglia derived from human embryonic stem cells. Microglia are very sensitive to culture conditions and therefore might only reflect partially *in vivo* microglia. In the *in vivo* studies, we have focused on mouse microglia. Their response to amyloid plaques is different from the response of human microglia.

STAR★METHODS

Detailed methods are provided in the online version of this paper and include the following:

- KEY RESOURCES TABLE
- RESOURCE AVAILABILITY
  - Lead contact
  - Materials availability
  - Data and code availability
- EXPERIMENTAL MODEL AND STUDY PARTICIPANT DETAILS
  - Mice
  - Primary human microglia
  - H9MG
  - HEK293T cell line
- METHOD DETAILS
  - Mice
  - Isolation of human and mouse primary microglia
  - RNA isolation, reverse transcription and real-time qPCR
  - Expression and validation of γ-secretase substrate candidates
  - Immunoblotting
  - Immunofluorescence staining of brain sections
  - Gamma-secretase Substrate Identification (G-SECSI) workflow
  - Preparation of **H9MG** single-cell samples
  - Single-cell mRNA **libraries** preparation and sequencing
- QUANTIFICATION AND STATISTICAL ANALYSIS
  - Quantitative analysis of the abundance of the CTFs
  - Functional and Pathway Enrichment Analysis of Candidate Substrates
  - Single-cell sequencing data analysis
  - Imaging and quantitative analysis of the Immunofluorescent images
- ADDITIONAL RESOURCES

AUTHOR CONTRIBUTIONS

P.H. and B.D.S. conceived and designed the study with the help of L.S., A.M.-M., M.F., and R.M. P.H. and B.D.S. wrote the first versions of the manuscript. P.H. performed experiments with help from L.S., A.M.-M., L.W., D.T., S.B., and R.M. and analyzed proteomics data with advice from L.S., M.F., R.M., A.J.M.H., and B.D.S. M.Z. and N.F. analyzed proteomics data and single-cell transcriptomics data with advice from P.H., A.M.-M., R.M., M.F., and B.D.S. L.W. prepared cDNA libraries for sequencing with assistance from S.P. T.T. provided tissues for human primary microglia isolation. L.S. generated *Aph1a*^{fl/fl}*b*[−/−]*c*[fl/fl] mouse strain (JAX stock #030985).[53] A.J.M.H. supervised all the MS sequencing-related work and processed the raw proteomics data. L.S., R.M., and B.D.S. supervised all the experiments. All authors discussed the results and commented on the manuscript.

DECLARATION OF INTERESTS

B.D.S. has been a consultant for Eli Lilly, Biogen, Janssen Pharmaceutica, Eisai, AbbVie, and other companies and is now a consultant for Eisai, Remynd, and Muna therapeutics. B.D.S. is a scientific founder of Augustine Therapeutics and a scientific founder and stockholder of Muna Therapeutics. R.M. has scientific collaborations with Alector, Nodthera, and Alchemab and has been a consultant for Sanofi.

INCLUSION AND DIVERSITY

We support inclusive, diverse, and equitable conduct of research.

(I–K) Quantitative analysis of microgliosis in the brain sections shown in (H). Coverage of microglia (EYFP$^+$) area (I) and density of microglial puncta (J, EYFP$^+$ puncta with diameter > 30 μm) per mm^2, and the ratio of overlapped microglia and plaque (EYFP$^+$82E1$^+$) area vs. total plaque (82E1$^+$) area (K) were quantified. (L) Quantitative analysis of Aβ plaques in the brain sections shown in (H). Ratio of Aβ plaques area per mm^2 was quantified. Data are shown as mean ± SEM. n = 5 animals in each condition. Each dot represents the average measurement value of two sections from an individual animal. p Values are determined by two-tailed unpaired Student's t test in (I)–(L).

REFERENCES

1. De Strooper, B. (2003). Aph-1, Pen-2, and Nicastrin with Presenilin generate an active γ-Secretase complex. Neuron *38*, 9–12. https://doi.org/10.1016/S0896-6273(03)00205-8.

2. Yang, G., Zhou, R., Guo, X., Yan, C., Lei, J., and Shi, Y. (2021). Structural basis of γ-secretase inhibition and modulation by small molecule drugs. Cell *184*, 521–533.e14. https://doi.org/10.1016/j.cell.2020.11.049.

3. De Strooper, B., Saftig, P., Craessaerts, K., Vanderstichele, H., Guhde, G., Annaert, W., Von Figura, K., and Van Leuven, F. (1998). Deficiency of presenilin-1 inhibits the normal cleavage of amyloid precursor protein. Nature *391*, 387–390. https://doi.org/10.1038/34910.

4. De Strooper, B., Annaert, W., Cupers, P., Saftig, P., Craessaerts, K., Mumm, J.S., Schroeter, E.H., Schrijvers, V., Wolfe, M.S., Ray, W.J., et al. (1999). A presenilin-1-dependent γ-secretase-like protease mediates release of notch intracellular domain. Nature *398*, 518–522. https://doi.org/10.1038/19083.

5. Habets, R.A., De Bock, C.E., Serneels, L., Lodewijckx, I., Verbeke, D., Nittner, D., Narlawar, R., Demeyer, S., Dooley, J., Liston, A., et al. (2019). Safe targeting of T cell acute lymphoblastic leukemia by pathology-specific NOTCH inhibition. Sci. Transl. Med. *11*. https://doi.org/10.1126/scitranslmed.aau6246.

6. De Strooper, B., and Annaert, W. (2010). Novel research horizons for presenilins and γ-secretases in cell biology and disease. Annu. Rev. Cell Dev. Biol. *26*, 235–260. https://doi.org/10.1146/annurev-cellbio-100109-104117.

7. Brown, M.S., Ye, J., Rawson, R.B., and Goldstein, J.L. (2000). Regulated intramembrane proteolysis: a control mechanism conserved from bacteria to humans. Cell *100*, 391–398. https://doi.org/10.1016/S0092-8674(00)80675-3.

8. Kopan, R., and Ilagan, M.X.G. (2004). γ-secretase: proteasome of the membrane? Nat. Rev. Mol. Cell Biol. *5*, 499–504. https://doi.org/10.1038/nrm1406.

9. Takami, M., Nagashima, Y., Sano, Y., Ishihara, S., Morishima-Kawashima, M., Funamoto, S., and Ihara, Y. (2009). γ-Secretase: successive tripeptide and tetrapeptide release from the transmembrane domain of β-carboxyl terminal fragment. J. Neurosci. *29*, 13042–13052. https://doi.org/10.1523/JNEUROSCI.2362-09.2009.

10. Güner, G., and Lichtenthaler, S.F. (2020). The substrate repertoire of γ-secretase/presenilin. Semin. Cell Dev. Biol. *105*, 27–42. https://doi.org/10.1016/j.semcdb.2020.05.019.

11. Zurhove, K., Nakajima, C., Herz, J., Bock, H.H., and May, P. (2008). γ-Secretase limits the inflammatory response through the processing of LRP1. Sci. Signal. *1*, ra15. https://doi.org/10.1126/scisignal.1164263.

12. Londino, J.D., Gulick, D., Isenberg, J.S., and Mallampalli, R.K. (2015). Cleavage of signal regulatory protein α (sirpα) enhances inflammatory signaling. J. Biol. Chem. *290*, 31113–31125. https://doi.org/10.1074/jbc.M115.682914.

13. Gulick, A.M. (2019). Enzymes engineered to trap reaction intermediates. Nature *565*, 28–29. https://doi.org/10.1038/d41586-018-07569-6.

14. Huguenin-Dezot, N., Alonzo, D.A., Heberlig, G.W., Mahesh, M., Nguyen, D.P., Dornan, M.H., Boddy, C.N., Schmeing, T.M., and Chin, J.W. (2019). Trapping biosynthetic acyl-enzyme intermediates with encoded 2,3-diaminopropionic acid. Nature *565*, 112–117. https://doi.org/10.1038/s41586-018-0781-z.

15. Tang, S., Beattie, A.T., Kafkova, L., Petris, G., Huguenin-Dezot, N., Fiedler, M., Freeman, M., and Chin, J.W. (2022). Mechanism-based traps enable protease and hydrolase substrate discovery. Nature *602*, 701–707. https://doi.org/10.1038/s41586-022-04414-9.

16. Wolfe, M.S. (2009). Intramembrane proteolysis. Chem. Rev. *109*, 1599–1612. https://doi.org/10.1021/cr8004197.

17. Zanotti, A., Coelho, J.P.L., Kaylani, D., Singh, G., Tauber, M., Hitzenberger, M., Avci, D., Zacharias, M., Russell, R.B., Lemberg, M.K., et al. (2022). The human signal peptidase complex acts as a quality control enzyme for membrane proteins. Science *378*, 996–1000. https://doi.org/10.1126/science.abo5672.

18. Blobel, G., and Dobberstein, B. (1975). Transfer of proteins across membranes: I. Presence of proteolytically processed and unprocessed nascent immunoglobulin light chains on membrane-bound ribosomes of murine myeloma. J. Cell Biol. *67*, 835–851. https://doi.org/10.1083/jcb.67.3.835.

19. Von Heijne, G. (1983). Patterns of amino acids near signal-sequence cleavage sites. Eur. J. Biochem. *133*, 17–21. https://doi.org/10.1111/j.1432-1033.1983.tb07424.x.

20. Petersen, T.N., Brunak, S., Von Heijne, G., and Nielsen, H. (2011). SignalP 4.0: discriminating signal peptides from transmembrane regions. Nat. Methods *8*, 785–786. https://doi.org/10.1038/nmeth.1701.

21. Struhl, G., and Adachi, A. (2000). Requirements for presenilin-dependent cleavage of notch and other transmembrane proteins. Mol. Cell *6*, 625–636. https://doi.org/10.1016/S1097-2765(00)00061-7.

22. Hemming, M.L., Elias, J.E., Gygi, S.P., and Selkoe, D.J. (2008). Proteomic profiling of γ-secretase substrates and mapping of substrate requirements. PLoS Biol. *6*, e257. https://doi.org/10.1371/journal.pbio.0060257.

23. Breimann, S., Kamp, F., Guner, G., Ortner, M., Lichtenthaler, S., Langosch, D., Frishman, D., and Steiner, H. (2022). Substrate-defining features of γ-secretase revealed by comparative physicochemical profiling and explainable AI. In 2nd International Meeting 2022 of the DFG-Research Unit 2290 "Understanding Intramembrane Proteolysis," p. 20.

24. Nimmerjahn, A., Kirchhoff, F., and Helmchen, F. (2005). Resting microglial cells are highly dynamic surveillants of brain parenchyma in vivo. Science *308*, 1314–1318. https://doi.org/10.1126/science.1110647.

25. Li, Q., and Barres, B.A. (2018). Microglia and macrophages in brain homeostasis and disease. Nat. Rev. Immunol. *18*, 225–242. https://doi.org/10.1038/nri.2017.125.

26. Giulian, D., Haverkamp, L.J., Yu, J.H., Karshin, W., Tom, D., Li, J., Kirkpatrick, J., Kuo, L.M., and Roher, A.E. (1996). Specific domains of β-amyloid from Alzheimer plaque elicit neuron killing in human microglia. J. Neurosci. *16*, 6021–6037. https://doi.org/10.1523/JNEUROSCI.16-19-06021.1996.

27. Wyss-Coray, T. (2006). Inflammation in Alzheimer disease: driving force, bystander or beneficial response? Nat. Med. *12*, 1005–1015. https://doi.org/10.1038/nm1484.

28. Hanisch, U.K., and Kettenmann, H. (2007). Microglia: active sensor and versatile effector cells in the normal and pathologic brain. Nat. Neurosci. *10*, 1387–1394. https://doi.org/10.1038/nn1997.

29. Salter, M.W., and Stevens, B. (2017). Microglia emerge as central players in brain disease. Nat. Med. *23*, 1018–1027. https://doi.org/10.1038/nm.4397.

30. Spangenberg, E., Severson, P.L., Hohsfield, L.A., Crapser, J., Zhang, J., Burton, E.A., Zhang, Y., Spevak, W., Lin, J., Phan, N.Y., et al. (2019). Sustained microglial depletion with CSF1R inhibitor impairs parenchymal plaque development in an Alzheimer's disease model. Nat. Commun. *10*, 3758. https://doi.org/10.1038/s41467-019-11674-z.

31. Huang, Y., Happonen, K.E., Burrola, P.G., O'Connor, C., Hah, N., Huang, L., Nimmerjahn, A., and Lemke, G. (2021). Microglia use TAM receptors to detect and engulf amyloid β plaques. Nat. Immunol. *22*, 586–594. https://doi.org/10.1038/s41590-021-00913-5.

32. Wunderlich, P., Glebov, K., Kemmerling, N., Tien, N.T., Neumann, H., and Walter, J. (2013). Sequential proteolytic processing of the triggering receptor expressed on myeloid cells-2 (TREM2) protein by ectodomain shedding and γ-secretase- dependent intramembranous cleavage. J. Biol. Chem. *288*, 33027–33036. https://doi.org/10.1074/jbc.M113.517540.

33. Jonsson, T., Stefansson, H., Steinberg, S., Jonsdottir, I., Jonsson, P.V., Snaedal, J., Bjornsson, S., Huttenlocher, J., Levey, A.I., Lah, J.J., et al. (2013). Variant of TREM2 associated with the risk of Alzheimer's disease. N. Engl. J. Med. *368*, 107–116. https://doi.org/10.1056/NEJMoa1211103.

34. Guerreiro, R., Wojtas, A., Bras, J., Carrasquillo, M., Rogaeva, E., Majounie, E., Cruchaga, C., Sassi, C., Kauwe, J.S.K., Younkin, S., et al. (2013). TREM2 variants in Alzheimer's disease. N. Engl. J. Med. *368*, 117–127. https://doi.org/10.1056/NEJMoa1211851.

35. Parhizkar, S., Arzberger, T., Brendel, M., Kleinberger, G., Deussing, M., Focke, C., Nuscher, B., Xiong, M., Ghasemigharagoz, A., Katzmarski, N., et al. (2019). Loss of TREM2 function increases amyloid seeding but reduces plaque-associated ApoE. Nat. Neurosci. *22*, 191–204. https://doi.org/10.1038/s41593-018-0296-9.

36. Krasemann, S., Madore, C., Cialic, R., Baufeld, C., Calcagno, N., El Fatimy, R., Beckers, L., O'Loughlin, E., Xu, Y., Fanek, Z., et al. (2017). The TREM2-APOE pathway drives the transcriptional phenotype of dysfunctional microglia in neurodegenerative diseases. Immunity *47*, 566–581.e9. https://doi.org/10.1016/j.immuni.2017.08.008.

37. Keren-Shaul, H., Spinrad, A., Weiner, A., Matcovitch-Natan, O., Dvir-Szternfeld, R., Ulland, T.K., David, E., Baruch, K., Lara-Astaiso, D., Toth, B., et al. (2017). A unique microglia type associated with restricting development of Alzheimer's disease. Cell *169*, 1276–1290.e17. https://doi.org/10.1016/j.cell.2017.05.018.

38. Doody, R.S., Raman, R., Farlow, M., Iwatsubo, T., Vellas, B., Joffe, S., Kieburtz, K., He, F., Sun, X., Thomas, R.G., et al. (2013). A phase 3 trial of semagacestat for treatment of Alzheimer's disease. N. Engl. J. Med. *369*, 341–350. https://doi.org/10.1056/NEJMoa1210951.

39. Mancuso, R., Fattorelli, N., Martinez-Muriana, A., Davis, E., Wolfs, L., Van den Daele, J., Geric, I., Preman, P., Serneels, L., and Poovathingal, S. (2022). A multi-pronged human microglia response to Alzheimer's disease Aβ pathology. bioRxiv.

40. Hasselmann, J., Coburn, M.A., England, W., Figueroa Velez, D.X., Kiani Shabestari, S., Tu, C.H., McQuade, A., Kolahdouzan, M., Echeverria, K., Claes, C., et al. (2019). Development of a chimeric model to study and manipulate human microglia in vivo. Neuron *103*, 1016–1033.e10. https://doi.org/10.1016/j.neuron.2019.07.002.

41. Mancuso, R., Van Den Daele, J., Fattorelli, N., Wolfs, L., Balusu, S., Burton, O., Liston, A., Sierksma, A., Fourne, Y., Poovathingal, S., et al. (2019). Stem-cell-derived human microglia transplanted in mouse brain to study human disease. Nat. Neurosci. *22*, 2111–2116. https://doi.org/10.1038/s41593-019-0525-x.

42. Tran, J.C., and Doucette, A.A. (2008). Gel-eluted liquid fraction entrapment electrophoresis: an electrophoretic method for broad molecular weight range proteome separation. Anal. Chem. *80*, 1568–1573. https://doi.org/10.1021/ac702197w.

43. Witkowski, C., and Harkins, J. (2009). Using the GELFREE 8100 Fractionation System for molecular weight-based fractionation with liquid phase recovery. J. Vis. Exp. *34*, e1842.

44. Willnow, T.E., Moehring, J.M., Inocencio, N.M., Moehring, T.J., and Herz, J. (1996). The low-density-lipoprotein receptor-related protein (LRP) is processed by furin in vivo and in vitro. Biochem. J. *313*, 71–76. https://doi.org/10.1042/bj3130071.

45. Bateman, A., Martin, M.J., Orchard, S., Magrane, M., Agivetova, R., Ahmad, S., Alpi, E., Bowler-Barnett, E.H., Britto, R., and Bursteinas, B. (2021). UniProt: the universal protein knowledgebase in 2021. Nucleic Acids Res. *49*, D480–D489. https://doi.org/10.1093/nar/gkaa1100.

46. Zhou, X., Wahane, S., Friedl, M.S., Kluge, M., Friedel, C.C., Avrampou, K., Zachariou, V., Guo, L., Zhang, B., He, X., et al. (2020). Microglia and macrophages promote corralling, wound compaction and recovery after spinal cord injury via Plexin-B2. Nat. Neurosci. *23*, 337–350. https://doi.org/10.1038/s41593-020-0597-7.

47. Sala Frigerio, C., Wolfs, L., Fattorelli, N., Thrupp, N., Voytyuk, I., Schmidt, I., Mancuso, R., Chen, W.T., Woodbury, M.E., Srivastava, G., et al. (2019). The major risk factors for Alzheimer's disease: age, sex, and genes modulate the microglia response to Aβ plaques. Cell Rep. *27*, 1293–1306.e6. https://doi.org/10.1016/j.celrep.2019.03.099.

48. Linnartz, B., and Neumann, H. (2013). Microglial activatory (immunoreceptor tyrosine-based activation motif)- and inhibitory (immunoreceptor tyrosine-based inhibition motif)-signaling receptors for recognition of the neuronal glycocalyx. Glia *61*, 37–46. https://doi.org/10.1002/glia.22359.

49. Linnartz, B., Wang, Y., and Neumann, H. (2010). Microglial immunoreceptor tyrosine-based activation and inhibition motif signaling in neuroinflammation. Int. J. Alzheimers Dis. *2010*. https://doi.org/10.4061/2010/587463.

50. Park, B.S., and Lee, J.O. (2013). Recognition of lipopolysaccharide pattern by TLR4 complexes. Exp. Mol. Med. *45*, e66. https://doi.org/10.1038/emm.2013.97.

51. Sousa, C., Golebiewska, A., Poovathingal, S.K., Kaoma, T., Pires-Afonso, Y., Martina, S., Coowar, D., Azuaje, F., Skupin, A., Balling, R., et al. (2018). Single-cell transcriptomics reveals distinct inflammation-induced microglia signatures. EMBO Rep. *19*, 1–17. https://doi.org/10.15252/embr.201846171.

52. Parkhurst, C.N., Yang, G., Ninan, I., Savas, J.N., Yates, J.R., Lafaille, J.J., Hempstead, B.L., Littman, D.R., and Gan, W.B. (2013). Microglia promote learning-dependent synapse formation through brain-derived neurotrophic factor. Cell *155*, 1596–1609. https://doi.org/10.1016/j.cell.2013.11.030.

53. Serneels, L., Dejaegere, T., Craessaerts, K., Horré, K., Jorissen, E., Tousseyn, T., Hébert, S., Coolen, M., Martens, G., Zwijsen, A., et al. (2005). Differential contribution of the three Aph1 genes to γ-secretase activity in vivo. Proc. Natl. Acad. Sci. USA *102*, 1719–1724. https://doi.org/10.1073/pnas.0408901102.

54. Friedman, B.A., Srinivasan, K., Ayalon, G., Meilandt, W.J., Lin, H., Huntley, M.A., Cao, Y., Lee, S.H., Haddick, P.C.G., Ngu, H., et al. (2018). Diverse brain myeloid expression profiles reveal distinct microglial activation states and aspects of Alzheimer's disease not evident in mouse models. Cell Rep. *22*, 832–847. https://doi.org/10.1016/j.celrep.2017.12.066.

55. Saito, T., Matsuba, Y., Mihira, N., Takano, J., Nilsson, P., Itohara, S., Iwata, N., and Saido, T.C. (2014). Single App knock-in mouse models of Alzheimer's disease. Nat. Neurosci. *17*, 661–663. https://doi.org/10.1038/nn.3697.

56. Glebov, K., Wunderlich, P., Karaca, I., and Walter, J. (2016). Functional involvement of γ-secretase in signaling of the triggering receptor expressed on myeloid cells-2 (TREM2). J. Neuroinflammation *13*, 17. https://doi.org/10.1186/s12974-016-0479-9.

57. Laurent, S.A., Hoffmann, F.S., Kuhn, P.H., Cheng, Q., Chu, Y., Schmidt-Supprian, M., Hauck, S.M., Schuh, E., Krumbholz, M., Rübsamen, H., et al. (2015). γ-secretase directly sheds the survival receptor BCMA from plasma cells. Nat. Commun. *6*, 7333. https://doi.org/10.1038/ncomms8333.

58. Vevea, J.D., Kusick, G.F., Courtney, K.C., Chen, E., Watanabe, S., and Chapman, E.R. (2021). Synaptotagmin 7 is targeted to the axonal plasma membrane through g-secretase processing to promote synaptic vesicle docking in mouse hippocampal neurons. eLife *10*. https://doi.org/10.7554/eLife.67261.

59. Güner, G., Aßfalg, M., Zhao, K., Dreyer, T., Lahiri, S., Lo, Y., Slivinschi, B.I., Imhof, A., Jocher, G., Strohm, L., et al. (2022). Proteolytically generated soluble Tweak Receptor Fn14 is a blood biomarker for γ-secretase activity. EMBO Mol. Med. *14*, e16084. https://doi.org/10.15252/emmm.202216084.

60. Weber, S., and Saftig, P. (2012). Ectodomain shedding and ADAMs in development. Development *139*, 3693–3709. https://doi.org/10.1242/dev.076398.

61. Wakabayashi, T., Craessaerts, K., Bammens, L., Bentahir, M., Borgions, F., Herdewijn, P., Staes, A., Timmerman, E., Vandekerckhove, J., Rubinstein, E., et al. (2009). Analysis of the γ-secretase interactome and validation of its association with tetraspanin-enriched microdomains. Nat. Cell Biol. *11*, 1340–1346. https://doi.org/10.1038/ncb1978.

62. Hur, J.Y., Frost, G.R., Wu, X., Crump, C., Pan, S.J., Wong, E., Barros, M., Li, T., Nie, P., Zhai, Y., et al. (2020). The innate immunity protein IFITM3 modulates γ-secretase in Alzheimer's disease. Nature *586*, 735–740. https://doi.org/10.1038/s41586-020-2681-2.

63. Myers, D.R., Zikherman, J., and Roose, J.P. (2017). Tonic signals: why do lymphocytes bother? Trends Immunol. *38*, 844–857. https://doi.org/10.1016/j.it.2017.06.010.

64. Roose, J.P., Diehn, M., Tomlinson, M.G., Lin, J., Alizadeh, A.A., Botstein, D., Brown, P.O., and Weiss, A. (2003). T cell receptor-independent basal signaling via Erk and Abl kinases suppresses RAG gene expression. PLoS Biol. *1*, E53. https://doi.org/10.1371/journal.pbio.0000053.

65. Tan, Y.X., Zikherman, J., and Weiss, A. (2013). Novel tools to dissect the dynamic regulation of TCR signaling by the kinase CSK and the phosphatase CD45. Cold Spring Harb. Symp. Quant. Biol. *78*, 131–139. https://doi.org/10.1101/sqb.2013.78.020347.

66. Gosselin, D., Skola, D., Coufal, N.G., Holtman, I.R., Schlachetzki, J.C.M., Sajti, E., Jaeger, B.N., O'Connor, C., Fitzpatrick, C., Pasillas, M.P., et al. (2017). An environment-dependent transcriptional network specifies human microglia identity. Science *356*. https://doi.org/10.1126/science.aal3222.

67. Lloyd, A.F., Martinez-Muriana, A., Hou, P., Davis, E., Mancuso, R., Brenes, A.J., Geric, I., Snellinx, A., Craessaerts, K., Theys, T., et al. (2022). Deep proteomic analysis of human microglia and model systems reveal fundamental biological differences of in vitro and ex vivo cells. bioRxiv, 1–30.

68. Deczkowska, A., Keren-Shaul, H., Weiner, A., Colonna, M., Schwartz, M., and Amit, I. (2018). Disease-associated microglia: A universal immune sensor of neurodegeneration. Cell *173*, 1073–1081. https://doi.org/10.1016/j.cell.2018.05.003.

69. Schlepckow, K., Monroe, K.M., Kleinberger, G., Cantuti-Castelvetri, L., Parhizkar, S., Xia, D., Willem, M., Werner, G., Pettkus, N., Brunner, B., et al. (2020). Enhancing protective microglial activities with a dual function TREM 2 antibody to the stalk region. EMBO Mol. Med. *12*, e11227. https://doi.org/10.15252/emmm.201911227.

70. De Strooper, B. (2014). Lessons from a failed γ-secretase Alzheimer trial. Cell *159*, 721–726. https://doi.org/10.1016/j.cell.2014.10.016.

71. Lichtenthaler, S.F., Lemberg, M.K., and Fluhrer, R. (2018). Proteolytic ectodomain shedding of membrane proteins in mammals—hardware, concepts, and recent developments. EMBO J. *37*. https://doi.org/10.15252/embj.201899456.

72. Esselens, C., Oorschot, V., Baert, V., Raemaekers, T., Spittaels, K., Serneels, L., Zheng, H., Saftig, P., De Strooper, B., Klumperman, J., et al. (2004). Presenilin 1 mediates the turnover of telencephalin in hippocampal neurons via an autophagic degradative pathway. J. Cell Biol. *166*, 1041–1054. https://doi.org/10.1083/jcb.200406060.

73. Annaert, W.G., Esselens, C., Baert, V., Boeve, C., Snellings, G., Cupers, P., Craessaerts, K., and De Strooper, B. (2001). Interaction with telencephalin and the amyloid precursor protein predicts a ring structure for presenilins. Neuron *32*, 579–589. https://doi.org/10.1016/S0896-6273(01)00512-8.

74. Serneels, L., Bammens, L., Zwijsen, A., Tolia, A., Chávez-Gutiérrez, L., and De Strooper, B. (2023). Functional and topological analysis of PSENEN, the fourth subunit of the γ-secretase complex. bioRxiv. 07.28.550932. https://doi.org/10.1101/2023.07.28.550932.

75. Mercken, M., Takahashi, H., Honda, T., Sato, K., Murayama, M., Nakazato, Y., Noguchi, K., Imahori, K., and Takashima, A. (1996). Characterization of human presenilin 1 using N-terminal specific monoclonal antibodies: evidence that Alzheimer mutations affect proteolytic processing. FEBS Lett. *389*, 297–303. https://doi.org/10.1016/0014-5793(96)00608-4.

76. Acx, H., Serneels, L., Radaelli, E., Muyldermans, S., Vincke, C., Pepermans, E., Müller, U., Chávez-Gutiérrez, L., and De Strooper, B. (2017). Inactivation of γ-secretases leads to accumulation of substrates

77. and non-Alzheimer neurodegeneration. EMBO Mol. Med. *9*, 1088–1099. https://doi.org/10.15252/emmm.201707561.

77. Hao, Y., Hao, S., Andersen-Nissen, E., Mauck, W.M., Zheng, S., Butler, A., Lee, M.J., Wilk, A.J., Darby, C., Zager, M., et al. (2021). Integrated analysis of multimodal single-cell data. Cell *184*, 3573–3587.e29. https://doi.org/10.1016/j.cell.2021.04.048.

78. van Wilgenburg, B., Browne, C., Vowles, J., and Cowley, S.A. (2013). Efficient, long term production of monocyte-derived macrophages from human pluripotent stem cells under partly-defined and fully-defined conditions. PLoS One *8*, e71098. https://doi.org/10.1371/journal.pone.0071098.

79. Bohlen, C.J., Bennett, F.C., Tucker, A.F., Collins, H.Y., Mulinyawe, S.B., and Barres, B.A. (2017). Diverse requirements for microglial survival, specification, and function revealed by defined-medium cultures. Neuron *94*, 759–773.e8. https://doi.org/10.1016/j.neuron.2017.04.043.

80. Yona, S., Kim, K.W., Wolf, Y., Mildner, A., Varol, D., Breker, M., Strauss-Ayali, D., Viukov, S., Guilliams, M., Misharin, A., et al. (2013). Fate mapping reveals origins and dynamics of monocytes and tissue macrophages under homeostasis. Immunity *38*, 79–91. https://doi.org/10.1016/j.immuni.2012.12.001.

81. Askew, K., Li, K., Olmos-Alonso, A., Garcia-Moreno, F., Liang, Y., Richardson, P., Tipton, T., Chapman, M.A., Riecken, K., Beccari, S., et al. (2017). Coupled proliferation and apoptosis maintain the rapid turnover of microglia in the adult brain. Cell Rep. *18*, 391–405. https://doi.org/10.1016/j.celrep.2016.12.041.

82. Schulz, C., Gomez Perdiguero, E.G., Chorro, L., Szabo-Rogers, H., Cagnard, N., Kierdorf, K., Prinz, M., Wu, B., Jacobsen, S.E.W., Pollard, J.W., et al. (2012). A lineage of myeloid cells independent of myb and hematopoietic stem cells. Science *336*, 86–90. https://doi.org/10.1126/science.1219179.

83. Wang, S., Sudan, R., Peng, V., Zhou, Y., Du, S., Yuede, C.M., Lei, T., Hou, J., Cai, Z., Cella, M., et al. (2022). TREM2 drives microglia response to amyloid-β via SYK-dependent and -independent pathways. Cell *185*, 4153–4169.e19. https://doi.org/10.1016/j.cell.2022.09.033.

84. Gowrishankar, K., Zeidler, M.G., and Vincenz, C. (2004). Release of a membrane-bound death domain by γ-secretase processing of the p75NTR homolog NRADD. J. Cell Sci. *117*, 4099–4111. https://doi.org/10.1242/jcs.01263.

85. Nakahara, S., Saito, T., Kondo, N., Moriwaki, K., Noda, K., Ihara, S., Takahashi, M., Ide, Y., Gu, J., Inohara, H., et al. (2006). A secreted type of β1,6 N-acetylglucosaminyltransferase V (GnT-V), a novel angiogenesis inducer, is regulated by γ-secretase. FASEB J. *20*, 2451–2459. https://doi.org/10.1096/fj.05-5066com.

86. Merrick, D., Chapin, H., Baggs, J.E., Yu, Z., Somlo, S., Sun, Z., Hogenesch, J.B., and Caplan, M.J. (2012). The γ-secretase cleavage product of Polycystin-1 regulates TCF and CHOP-mediated transcriptional activation through a p300-dependent mechanism. Dev. Cell *22*, 197–210. https://doi.org/10.1016/j.devcel.2011.10.028.

87. Meyer, E.L., Strutz, N., Gahring, L.C., and Rogers, S.W. (2003). Glutamate receptor subunit 3 is modified by site-specific limited proteolysis including cleavage by γ-secretase. J. Biol. Chem. *278*, 23786–23796. https://doi.org/10.1074/jbc.M301360200.

88. De Rop, F.V., Ismail, J.N., Bravo González-Blas, C.B., Hulselmans, G.J., Flerin, C.C., Janssens, J., Theunis, K., Christiaens, V.M., Wouters, J., Marcassa, G., et al. (2022). HyDrop enables droplet based single-cell ATAC-seq and single-cell RNA-seq using dissolvable hydrogel beads. eLife *11*. https://doi.org/10.7554/eLife.73971.

STAR★METHODS

KEY RESOURCES TABLE

REAGENT or RESOURCE	SOURCE	IDENTIFIER
Antibodies		
Anti-APP-c20 (B63.3)	De Strooper's lab,[72] KU Leuven	N/A
Anti-PSEN1-NTF (B19)	De Strooper's lab,[73] KU Leuven	N/A
Anti-APH1A-CTF (B80.3)	De Strooper's lab,[53] KU Leuven	N/A
Anti-Nicastrin (9C3)	De Strooper's lab,[72] KU Leuven	N/A
Anti-PEN2-NTF (B126)	De Strooper's lab,[74] KU Leuven	N/A
Anti-hPSEN1-NTF (MKAD 3.5)	Marc Mercken,[75] Mitsubishi Kasei Institute of Life Sciences	N/A
Anti-PSEN2-CTF (D30G3)	Cell Signaling Technology	Cat#9979; RRID:AB_10829910
Anti-APH1B (Anti-APH1b/c)(L82)	De Strooper's lab,[76] KU Leuven	N/A
Anti-APLP2 (W2CT)	David Walsh University College Dublin	N/A
Anti-Syndecan 3 (2E9)	Guido David, KU Leuven	N/A
Anti-LRP1 (EPR3724)	Epitomics	Cat#2703-1
Anti-GAPDH	HyTest	Car#5G4-6C5; RRID:AB_1616722
Anti-β-ACTIN	Sigma	Cat#A5441; RRID:AB_476744
Anti-ATP1A1	Novus Bio	Cat#NB300-146; RRID:AB_2060979
Anti-FLAG (M2)	Sigma	Cat#F3165; RRID:AB_259529
Anti-GFP	Abcam	Cat#Ab13970; RRID:AB_300798
Anti-Amyloid β (N) (82E1)	IBL	Cat#10323; RRID:AB_1630806
Goat anti-mouse IgG-HRP	Bio-Rad	Cat#170-6516; RRID:AB_11125547
Goat anti-rabbit IgG-HRP	Bio-Rad	Cat#170-6515; RRID:AB_11125142
Donkey anti-mouse IgG-AF647	Invitrogen	Cat#A31571; RRID:AB_162542
Donkey anti-chicken IgG-AF488	Jackson Immunolabs	Cat#703-545-155; RRID:AB_2340375
Anti-human CD11b MicroBeads	Miltenyi	Cat#130-093-634
Anti-mouse CD11b-PE (REA592)	Miltenyi	Cat#130-113-806; RRID:AB_2751172
Anti-mouse CD45-BV421	BD Biosciences	Cat#563890; RRID:AB_2651151
Anti-mouse Hashtag 1 (A0301)	BioLegend	Cat#155801; RRID:AB_2750032
Anti-mouse Hashtag 2 (A0302)	BioLegend	Cat#155803; RRID:AB_2750033
Anti-mouse Hashtag 3 (A0303)	BioLegend	Cat#155805; RRID:AB_2750034
Anti-mouse Hashtag 4 (A0304)	BioLegend	Cat#155807; RRID:AB_2750035
Anti-human Hashtag 1 (A0251)	BioLegend	Cat#394601; RRID:AB_2750015
Anti-human Hashtag 2 (A0252)	BioLegend	Cat#394603; RRID:AB_2750016
Anti-human Hashtag 3 (A0253)	BioLegend	Cat#394605; RRID:AB_2750017
Anti-human Hashtag 4 (A0254)	BioLegend	Cat#394607; RRID:AB_2750018
Anti-human Hashtag 5 (A0255)	BioLegend	Cat#394609; RRID:AB_2750019
Anti-human Hashtag 6 (A0256)	BioLegend	Cat#394611; RRID:AB_2750020
Anti-human Hashtag 7 (A0257)	BioLegend	Cat#394613; RRID:AB_2750021
Anti-human Hashtag 8 (A0258)	BioLegend	Cat#394615; RRID:AB_2750022
Anti-human Hashtag 9 (A0259)	BioLegend	Cat#394617; RRID:AB_2750023
Anti-human Hashtag 10 (A0260)	BioLegend	Cat#394619; RRID:AB_2750024
Anti-human Hashtag 12 (A0262)	BioLegend	Cat#394623; RRID:AB_2750025
Anti-human Hashtag 13 (A0263)	BioLegend	Cat#394625; RRID:AB_2750026
Biological Samples		
Human brain tissue	Tom Theys, UZ Leuven	https://www.uzleuven.be/nl

(Continued on next page)

Continued

REAGENT or RESOURCE	SOURCE	IDENTIFIER
Chemicals, Peptides, and Recombinant Proteins		
Semagacestat	Jassen Pharmaceuticals	LY-450139
Tamoxifen	Sigma	Cat#T5648-1G
Rock inhibitor	Sigma	Cat#Y-27632
L-Glutamine	Sigma	Cat#G7513
N-acetyl-L-cysteine	Sigma	Cat#A7250
Human insulin	Sigma	Cat#I9278
Apo-transferrin	Sigma	Cat#T1147
Sodium selenite	Sigma	Cat#S9133
Cholesterol	Sigma	Cat#C4951
Heparin sulfate	Ams bio UK	Cat#GAG-HS01
Recombinant Human BMP4	Peprotech	Cat#120-05
Recombinant Human SCF	Peprotech	Cat#300-07
Recombinant Human VEGF	Peprotech	Cat#100-20
Recombinant Human M-CSF	Peprotech	Cat#300-25
Recombinant Human IL-3	Peprotech	Cat#200-03
Recombinant Human IL34	Peprotech	Cat#200-34
TGFβ1	Peprotech	Cat#100-21
CX3CL1	Peprotech	Cat#300-31
SuperScript™ II Reverse Transcriptase	Invitrogen	Cat#18064
Oligo(dT)12-18	Invitrogen	Cat#18418012
RNaseOUT™	Invitrogen	Cat#10777-019
dNTP Mix	Invitrogen	Cat#18427089
DTT	Sigma	Cat#3483-12-3
SensiFAST Sybr No Rox Mix 2x	Meridian	Cat#BIO-98005
Percoll	GE Healthcare	Cat#17-5445-02
Red Blood Cell Lysis Buffer	Biolegend	Cat#420301
Fixable Viability Dye eFluor™ 506/780	eBioscience	Cat#65-2860-40
Actinomycin D	Sigma	Cat#A1410
Protease inhibitor cocktail	Roche	Cat#11697498001
Critical Commercial Assays		
Neural Tissue Dissociation Kit (P)	Miltenyi	Cat#130-092-628
RNeasy® Micro Kit	QIAGEN	Cat#74004
Bradford Protein Assay	Bio-Rad	Cat#5000001
TransIT®-LT1 Transfection Reagent	Mirus	Cat#MIR 2305
GELFREE 8100 10% Cartridge Kit	Expedeon	Cat#SKU 42105
Single-cell gene expression profiling kit	10X Genomics	Cat#CG000204_ChromiumNext GEMSingleCell3_v3.1
Deposited Data		
Original images and blots	This paper	Mendeley Data [https://doi.org/10.17632/kgzzfrm272.1]
Proteomics dataset	This paper	ProteomeXchange [PXD039238]
Single-cell dataset	This paper	GEO [GSE245391]
Transcriptomics dataset	Mancuso et al.[41]	GEO [GSE137444]
Transcriptomics dataset	Sala Frigerio et al.[47]	GEO [GSE127893]
Transcriptomics dataset	Hasselman et al.[40]	GEO [GSE133433]
Transcriptomics dataset	Keren-Shaul et al.[37]	GEO [GSE98969]
Transcriptomics dataset	Friedman et al.[54]	GEO [GSE89482]

Continued

REAGENT or RESOURCE	SOURCE	IDENTIFIER
Experimental Models: Cell Lines		
H9 stem cell line	De Strooper's lab	WAe009-A; https://hpscreg.eu/cellline/WAe009-A
HEK293T/17	ATCC	Cat#CRL-11268
Experimental Models: Organisms/Strains		
Mouse: *C57BL/6J*	The Jackson Laboratory	Cat#000664
Mouse: *App^NL-G-F*	Takaomi Saido,[55] RIKEN Center for Brain Science	N/A
Mouse: *Cx3cr1^CreERT2/WT*	The Jackson Laboratory[52]	Cat#021160
Mouse: *Aph1a^fl/fl b^-/- c^fl/fl*	De Strooper's lab[53]	Cat#030985
Mouse: *Cx3cr1^CreERT2/WT* x *Aph1a^fl/fl b^-/- c^fl/fl*	This paper	N/A
Mouse: *Cx3cr1^CreERT2/WT* x *Aph1a^fl/fl b^-/- c^fl/fl* x *App^NL-G-F*	This paper	N/A
Oligonucleotides		
See Table S4 for Primer pairs of qPCR	This paper	N/A
Recombinant DNA		
pcDNA3.1+ hTNFRSF1B/C-(K)DYK	GenScript	Cat#OHU19055D
pcDNA3.1+ hCD300A/C-(K)DYK	GenScript	Cat#OHU05929D
pcDNA3.1+ hMILR1/C-(K)DYK	GenScript	Cat#OHu15096D
pLKO.1-puro-CMV-TurboGFP™	Sigma	Cat#SHC003
Software and Algorithms		
ImageJ	NIH	https://imagej.nih.gov/ij/
Image Studio Lite Ver 5.2	LI-COR	https://www.licor.com/bio/image-studio/
Prism 9	GraphPad	https://www.graphpad.com/scientificsoftware/prism/
FCS Express 7	De Novo Software	https://denovosoftware.com/
NIS-Elements AR (5.41.01)	Nikon	https://www.microscope.healthcare.nikon.com/en_AOM/products/software/nis-elements
Inkscape (0.92.4)	"Inkscape's Contributors" and "The Inkscape Project"	https://inkscape.org/
GIMP (2.10.18)	GNU Image Manipulation Program	https://www.gimp.org/
BioRender	BioRender	https://www.biorender.com/
R (v4.1.0)	R Core Team and the R Foundation for Statistical Computing	https://www.r-project.org/
Cell Ranger (v6.0.1)	10x Genomics	https://support.10xgenomics.com/single-cell-gene-expression/software/
Seurat (v4.0)	Satija lab[77]	https://satijalab.org/seurat/
MaxQuant (v 1.6.10.43)	MaxQuant	https://www.maxquant.org/

RESOURCE AVAILABILITY

Lead contact

Further information and requests for resources and reagents should be directed to and will be fulfilled by the lead contact, Bart De Strooper (bart.destrooper@kuleuven.be).

Materials availability

Materials and reagents used in this study are listed in the key resources table. Reagents generated in this study are available upon request.

Data and code availability

- Mass spectrometry data files and MaxQuant analysis files generated in this study have been deposited at the ProteomeXchange data repository and are publicly available as of the date of publication. The accession number is indicated in the key resources table. Please notice that the fraction 2-13 in the raw data are referring to the fraction 1-12 in the figures in this paper, since the first fraction generated from the GELFREE 8100 Fractionation System was not included for further analysis according to the manufacturer's recommendations. Single-cell RNA-seq data files generated in this study have been deposited at Gene Expression Omnibus (GEO) database and are publicly available as of the date of publication. The accession number is indicated in the key resources table. This paper analyzes existing, publicly available data. The accession numbers for the data-sets are listed in the key resources table. Original western blot images and microscopy data have been deposited at Mendeley Data and are publicly available as of the date of publication. The DOI is listed in the key resources table.
- This paper does not report original code.
- Any additional information required to reanalyze the data reported in this paper is available from the lead contact upon request.

EXPERIMENTAL MODEL AND STUDY PARTICIPANT DETAILS

Mice

C57BL/6J mice (JAX stock #000664), App^{NL-G-F} mice (obtained from Dr. Takaomi Saido),[55] $Cx3cr1^{CreERT2/wt}$ mice (JAX stock #021160)[52] and $Aph1a^{fl/fl}b^{-/-}c^{fl/fl}$ mice (JAX stock #030985)[53] were bred and maintained in local facilities. $Cx3cr1^{CreERT2/wt}$ mice and $Aph1a^{fl/fl}b^{-/-}c^{fl/fl}$ mice were crossed to generate the tamoxifen-inducible microglia-specific γ-secretase conditional KO mice ($Cx3cr1^{CreERT2/wt}$ x $Aph1a^{fl/fl}b^{-/-}c^{fl/fl}$). This strain was further crossed with App^{NL-G-F} mice to generate the mice with AD background ($Cx3cr1^{CreERT2/wt}$ x $Aph1a^{fl/fl}b^{-/-}c^{fl/fl}$ x App^{NL-G-F}). 3-month-old $Cx3cr1^{CreERT2/wt}$ x $Aph1a^{fl/fl}b^{-/-}c^{fl/fl}$ mice, 3-month-old and 7-month-old $Cx3cr1^{CreERT2/wt}$ x $Aph1a^{fl/fl}b^{-/-}c^{fl/fl}$ x APP^{NL-G-F} mice were used for the single-cell RNA sequencing experiment. 6-Month-old $Cx3cr1^{wt/wt}$ x $Aph1a^{fl/fl}b^{-/-}c^{fl/fl}$ x APP^{NL-G-F} mice were used for tamoxifen control. 5-month-old C57BL/6J mice were used for detection of γ-secretase subunits in microglia. Both female and male animals were used in experiments. Littermates of the same sex were randomly assigned to experimental groups. Mice were housed in groups of 2-4, under a 14 h light (7 am to 9 pm) and 10 h dark cycle at 21°C, with food and water *ad libitum*. All experiments were conducted according to protocols approved by the local Ethical Committee of Laboratory Animals of the KU Leuven (government license LA1210579, ECD project number P177/2020) following local and EU guidelines.

Primary human microglia

For human microglia isolation, temporal neocortex tissues were obtained from a 2-year old male (Caucasian) and a 22-year old female (Caucasian) patient. Both patients were diagnosed with epilepsy and underwent a neurosurgical resection at UZ Leuven. Samples were collected at the time of surgery and transferred on ice to the laboratory for tissue processing within 10 min post-sampling. All procedures were conducted in accordance with the protocols approved by the local Ethical Committee (protocol number S61186).

H9MG

We used *in vitro* human microglia-like cells generated from H9 embryonic stem cells (WA09, purchased from WiCell) according to the serum- and feeder-free protocol for hPSC-derived monocytes/macrophages.[78] Bohlen et al. optimized microglia medium conditions and developed TIC medium that mainly contains three astrocyte-derived key components TGF-β, IL-34 and cholesterol.[79] We adapted these two protocols described above to generate H9MG (Figure S1).

Briefly, H9 embryonic stem cells were expanded in Essential 8 medium with its supplement (A1517001, Gibco) in matrigel-coated 6-well plates. At day 0, H9 stem cells were dissociated with Accutase (A6964, Sigma-Aldrich) and suspended in mTeSR-1 medium with its supplement (#85850, Stemcell Technologies). Then, ~1 million cells were seeded in a 96-well u-bottom ultra-low adherence plate (#650979, Greiner Bio-one) and supplemented with Rock inhibitor (Y-27632, Sigma-Aldrich) and cytokines (50 ng/mL BMP4, 20 ng/mL SCF and 50 ng/mL VEGF). We spun the plate at 100 g for 3 minutes to pellet cells on the bottom of the wells. From day 1 to day 3, the medium was daily changed. At day 4, embryonic bodies (EBs) were collected from the plates and transferred to a T175 flask. Each flask contained 192 EBs in 40 mL differentiation medium (X-VIVO15, 100 ng/mL M-CSF, 25 ng/mL IL3, 2 mM Glutamax, 100 U/mL Pen/Strep and 0.055 mM β-mercaptoethanol). The differentiation medium was changed when it got yellow. From day 18 onward, the H9-derived monocyte-like cells (H9MC) were visible in the supernatant, and the non-adherent H9MC could be collected weekly. All the H9MC used in this study were collected from day 18, day 25 and day 32. The harvested H9MC were then transferred to the microglia TIC medium (DMEM F12, 2 mM L-Glutamine, 5 μg/mL N-acetyl-L-cysteine, 5 μg/mL human insulin, 100 μg/mL apo-transferrin, 100 ng/mL sodium selenite, 1.5 μg/mL cholesterol, 1 μg/mL heparin sulfate, 50 ng/mL M-CSF, 50 ng/mL IL34, 25 ng/mL TGFβ1, 10 ng/mL CX3CL1) for 7-day further maturation to H9MG. All cytokines used in this study were purchased from Peprotech. Using this combined protocol, we were able to generate ≥ 300 million H9MG in a T175 flask within 39 days.

HEK293T cell line

HEK293T cells were cultured in Dulbecco's modified Eagle's medium/F-12 (Invitrogen), 10% fetal bovine serum (GIBCO). Cells were maintained in a humidified incubator at 37°C with 5% CO2.

METHOD DETAILS

Mice

While $Cx3cr1^{CreERT2/WT}$ targets not only microglia but also other myeloid linage cells,[80] for instance circulating monocytes, the tamoxifen inducible recombinase activity[52] allows us to induce the KO after embryo development (1 month old in this study) and analyse the cells months later (2-6 month later in this study). Microglia originate from the yolk sac and self-renew in the brain,[81,82] while monocytes derive from bone-marrow and undergo fast turnover. Several studies have shown that the Cre modified monocytes can be replaced within 1 month upon withdraw of tamoxifen but Cre modified microglia stay permanently in the brain.[52,83] Therefore, mice were treated with tamoxifen (single dose of 2 mg /kg per day) or vehicle (corn oil) by i.p. injection for 5 consecutive days at 1 month of age and sacrificed at the indicated time points. For mouse microglia isolation and histology, mice were terminally anesthetized with an overdose of sodium pentobarbital and transcardially perfused with heparinized PBS.

Isolation of human and mouse primary microglia

The procedures of human and mouse primary microglia isolation are as previously described.[41] Briefly, tissues were subjected to dissociation using the Neural Tissue Dissociation Kit (P) (#130-092-628, Miltenyi) following the manufacturer's specifications. The cell suspension was filtered over a 70-μm cell strainer (#542070, Greiner) with ice-cold FACS buffer (PBS, 2% FCS, 2 mM EDTA). The filtered suspension was further centrifuged at 300g at 4 °C for 15 min. We suspended the cell pellet with 30% Percoll (#17-5445-02, GE Healthcare) and spun the suspension at 300g at 4 °C for 15 min. Myelin layers were formed on top of the supernatant and were removed with a Pasteur pipette.

For human microglia isolation, the cell pellets were first suspended in 1x Red Blood Cell Lysis Buffer (#420301, Biolegend) and incubated for 5 min on ice with occasional shaking. Then, the reaction was stopped by diluting with sufficient ice-cold PBS. The cell suspension was centrifuged at 300g at 4 °C for 15 min, and pellets were suspended in FACS buffer with anti-human CD11b MicroBeads (1:10, #130-093-634, Miltenyi) at 4 °C for 15 min. Microglia were washed and sorted on a Miltenyi MACS Magnetic Separator. CD11b positive fraction (microglia) and CD11b negative fraction (non-microglia cell types) were collected separately. Western blot analysis was performed for the quality control of microglia purity (not shown). At the end, ∼1.5 million human primary microglia were collected from each tissue sample and lysed for detection of γ-secretase subunits.

For mouse microglia isolation, the cell pellet was suspended in FACS buffer with anti-mouse CD11b-PE (1:50, REA592, Miltenyi), anti-mouse CD45-BV421 (1:500, #563890, BD Biosciences) and the cell viability marker e780 (1:2000, #65-2860-40, eBioscience) and incubated at 4 °C for 30 min. For the single-cell experiments, we added a specific hashtag antibody (A0301-A0304, Biolegend) for each individual sample during the antibody incubation. Microglia were washed and sorted on a Miltenyi MACSQuant Tyto cell sorter. Alive microglia expressing CD11b and medium level CD45 but e780 negative were sorted (not shown). At the end, ∼2 million microglia sorted from equally pooled brain cell suspension from three $C57BL/6J$ mice were lysed for detection of γ-secretase subunits (WB). ∼15,000 microglia from each GS^{KO}, GS^{WT}, TAM_QC or $Ctrl\_QC$ mouse were sorted for the single-cell mRNA library preparation. FACS data were analyzed using FCS express software.

RNA isolation, reverse transcription and real-time qPCR

RNA from different stages of microglia-like cell differentiation was isolated using the RNeasy Micro Kit (#74004, QIAGEN) according to the manufacturer's instructions. Reverse transcription of 200 ng (mRNA) from each sample was performed using the Superscript II reverse transcriptase (#18064, Invitrogen) according to the manufacturer's instructions. Real-time semi-quantitative PCR was performed using the SensiFast Sybr No-Rox kit (BIO-98020, Bioline). All qPCR primers are indicated in Table S4. Mean expression of two housekeeping genes (18S and GAPDH) was used for all normalizations. The expression level of the genes are shown in ΔCt.

Expression and validation of γ-secretase substrate candidates

HEK293T cells were transiently transfected with the recombinant plasmids pcDNA3.1+ hTNFRSF1B/C-(K)DYK, pcDNA3.1+ hCD300A/C-(K)DYK, pcDNA3.1+ hMILR1/C-(K)DYK and the positive transfection control pLKO.1-puro-CMV-TurboGFP, separately, using TransIT®-LT1 Transfection Reagent (Mirus). 36 hours after the transfection, cells were treated with 90 nM Semagacestat or DMSO for 16 hours and then collected for immunoblotting analysis using a FLAG M2 antibody (Sigma).

Immunoblotting

Cells for western blotting were washed in ice-cold PBS and then lysed in STE buffer (250 mM sucrose, 5 mM Tris-HCL, 1 mM EGTA, pH7.4) supplemented with protease inhibitor (Roche) and 1% Triton X-100 (Sigma) for 20 minutes in ice. Cell extract was centrifuged at 14, 000 rpm for 20 min and supernatant was collected and subjected to protein concentration measurement. Equal amount of protein in each sample mixed with NuPAGE LDS Sample Buffer (Invitrogen) was loaded on 4 to 12% Bis-Tris gels for SDS-PAGE. Resolved proteins were transferred on PVDF membranes. Membranes were blocked in 5% skimmed milk in TBS with 0.1% Tween

20 at RT for 45 minutes. The following primary antibodies were used in the study: APP-c20 (B63.3), PSEN1-NTF (B19), APH1A-CTF (B80.3), NCT (9C3), PEN2-NTF (B126) have been described.[53,72–74] PSEN1-NTF (1:1,000, MKAD 3.5) was a gift from Marc Mercken; PSEN2 (1:1,000, D30G3, Cell Signaling); APH1B (human) or APH1b/c (mouse) (1:1,000, L82) was generated in the laboratory by immunizing rabbits with a QDKNFLLYNQRSR peptide[76]; APLP2 (1:1,000, W2CT) was a gift from D. Walsh, and Syndecan3 (1:1,000, 2E9) was a gift from G. David; LRP1 (1:15,000, EPR3724, Epitomics), GAPDH (1:10,000, 5G4, HyTest); β-ACTIN (1:10,000, A5441, Sigma). ATP1A1 (1:1,000, NB300-146, Novus Bio); FLAG M2 (1:1,000, F3165, Sigma). The membrane was incubated with primary antibody solution at 4 °C overnight. Then we washed the membrane with TBST 3 times and incubated it with the HRP-labeled secondary antibody at RT for 1h. Secondary antibodies are goat polyclonal anti-mouse IgG-HRP conjugate (1:10,000, #170-6516, Bio-Rad), goat polyclonal anti-rabbit IgG-HRP conjugate (1:10,000, #170-6515, Bio-Rad). We washed the membrane with TBST 3 times and TBS 2 times. Eventually, blots were imaged by using the ImageQuant LAS 4000 mini biomolecular imager (GE Healthcare).

Immunofluorescence staining of brain sections
The PBS perfused mouse brain samples were fixed overnight with 4% PFA in PBS. Brains were then embedded in 4% Top Vision low-meltingpoint agarose (Thermo Fisher Scientific) and cut into 35 μm thick coronal sections using a vibratome (Leica VT1000S). The sections were blocked and permeabilized in a PBS based buffer supplemented with 5% donkey serum and 0.3% triton x100 for 1.5 hours at room temperature. After blocking, the sections were incubated in the blocking buffer based primary antibody solution (GFP (1:1,000, Ab13970, abcam); 82E1 (1:200, #10323, IBL)) gently agitated overnight at 4°C. The next day, sections were washed three times for 5 minutes in PBST (0.3% triton x100 in PBS). The sections were incubated with the blocking buffer based secondary antibody solution (Donkey anti-mouse AF647 (1:500, A31571, Invitrogen) and Donkey anti-chicken AF488 (1:500, 703-545-155, Jackson Immunolabs)) gently agitated for two hours at room temperature. The sections were then stained with DAPI solution (1/5,000 in PBS) gently agitated for 15 minutes at room temperature. Finally, the sections were washed three times for 5 minutes in PBST and mounted onto glass slides using the Glycergel mounting media and allowed to dry at room temperature.

Gamma-secretase Substrate Identification (G-SECSI) workflow
Step 1. γ-secretase Inhibition
Semagacestat was solubilized in DMSO and then diluted in the culture medium with final DMSO dilution by volume 1/1000. At day 6 in TIC, H9MG were refreshed with 2 μM Semagacestat containing microglia TIC medium for 16 hours. H9MG cultured in TIC medium containing 0.1% DMSO were used as control.

Step 2. Membrane protein purification
Cells were washed twice with ice-cold washing buffer (PBS supplemented with protease inhibitor cocktail (#11697498001, Roche)). Then, cells were mechanically detached from the dishes or flasks with a cell scraper and collected in ice-cold washing buffer. Cells were pelleted by centrifugation at 800g for 10 min and re-suspended with STE buffer (250 mM sucrose, 5 mM Tris-HCL, 1 mM EGTA, pH7.4) supplemented with protease inhibitor without detergent. 10 μL STE buffer was used per mg pellet. Then, we used a cell cracker with a bead of 8.010 mm diameter to homogenize the cells. Cell suspension was pushed through the cracker with syringes (20 times) to achieve a complete homogenization. Cell homogenate was centrifuged at 800g for 10 min to remove nuclei, and subsequently the supernatant was spun at 15,000g for 10 min to reduce the mitochondria content. Then, the remaining supernatant was collected and spun at 100,000g for 1 h to pellet the membrane fraction. The membrane pellet was washed with 100 mM Na_2CO_3 (pH 11.3) for 10 min and was spun at 100,000g for 0.5 h to pellet the membranes again. All steps were done at 4°C or on ice.

Step 3. Molecular weight-based protein fractionation and quality control
Molecular weight-based protein fractionation. The membrane pellets were re-suspended in STE buffer without detergent, and the protein concentrations were determined using a Bradford Protein Assay (Bio-Rad). To fractionate membrane proteins by their molecular weights, we used GELFREE 8100 Fractionation System with a GELFREE 8100 10% Cartridge Kit (SKU 42105, Expedeon) following the manufacturer's recommendations. Briefly, purified membrane proteins were mixed with Sample Buffer (from the kit) supplemented with 1M DTT (#3483-12-3, Sigma) and heated at 95°C for 5 min for denaturation. Then, samples were cooled down and loaded. 4 channels of the cartridge were used for each pair of samples (Semagacestat treated and control) from each batch, with 300 μg membrane proteins loaded in each channel and 2 channels for each sample. Then, the cartridge was placed on the instrument, and the fractionation programme as indicated in Table S5 was started. During each pause of the procedure, protein fractions in the collection chambers were transferred by using a multichannel pipette and collected in clean Eppendorf tubes on ice. The collection chambers were washed twice by using Running Buffer (from the Kit). After the washing, 100 μL fresh Running Buffer was added to the collection chamber, and the fractionation programme was continued. The first fraction collected during the first pause of the programme was discarded as the manufacturer suggested, since it contains mainly small debris. Finally, twelve fractions from each sample were collected and stored at -80°C.

Ponceau staining and Western blotting. Membrane protein (1 μg) from the whole purified membrane protein lysate as well from each fraction generated by GELFREE 8100 fractionation system was loaded on a 4-12% NuPAGE Bis-Tris gel (NP0323BOX, ThermoFisher) for SDS-PAGE. After transfer to a nitrocellulose membrane, we performed Ponceau staining. After 1 min staining, the membrane was washed 3 times with distilled water and was then imaged. The membrane was incubated in blocking buffer

(5% skimmed milk powder in TBS with 0.1% Tween 20) at RT for 45 min. We first probed the membrane with a primary C-terminal specific antibody against LRP1 (EPR3724, Epitomics). The membrane was incubated with primary antibody solution at 4 °C overnight. Then we washed the membrane with TBST 3 times and incubated it with the HRP-labeled secondary antibody at RT for 1h. We washed the membrane with TBST 3 times and TBS 2 times. Eventually, blots were imaged by using the ImageQuant LAS 4000 mini biomolecular imager (GE Healthcare).

Step 4. MS and CTF identification

Sample preparation for mass spectrometry.   H9MG fractionated membrane samples were prepared for mass spectrometry using s-trap mini columns (Protifi). Membrane pellets were solubilized in 5% SDS, 10mM TCEP (tris (2-carboxyethyl) phosphine) and 50mM TEAB (triethylammonium bicarbonate). Samples were alkylated with 20 mM iodoacetamide for 1 hour. Samples were loaded onto s-trap columns following the manufacturer's instructions and columns were washed 5 times with 100mM TEAB pH 7.1 in 90% methanol. Proteins were digested with trypsin (1:20 enzyme to protein) in 100 mM ammonium bicarbonate at 47 °C for 2 hours. Peptides were eluted from the mini column by sequential washes with 80ul 100mM ammonium bicarbonate followed by 80ul 0.2% formic acid and lastly with 80ul 0.2% formic acid in 50% acetonitrile. Peptides were dried and suspended in 45μl of 1% formic acid for analysis by mass spectrometry.

Liquid chromatography mass spectrometry analysis.   H9MG membrane derived peptides were analyzed using an Exploris 480 (Thermo Scientific) mass spectrometer coupled with a Dionex Ultimate 3000 RS (Thermo Scientific). LC buffers were the following: buffer A (0.1% formic acid in Milli-Q water (v/v)) and buffer B (80% acetonitrile and 0.08% formic acid in Milli-Q water (v/v). For all samples 15 μL of the suspended peptides was loaded at 10 μL/min onto a trap column (100 μm × 2 cm, PepMap nanoViper C18 column, 5 μm, 100 Å, Thermo Scientific) equilibrated in 2% buffer B. The trap column was washed for 5 min at the same flow rate and then the trap column was switched in-line with a Thermo Scientific, resolving C18 column (75 μm × 50 cm, PepMap RSLC C18 column, 2 μm, 100 Å). Peptides were eluted from the column at a constant flow rate of 300 nl/min with a linear gradient from 5% buffer B to 35% buffer B in 125 min and then to 98% buffer B by 127 min. The column was then washed with 98% buffer B for 20 min. The data was acquired using an easy spray source operated in positive mode with spray voltage at 2.6 kV, and the ion transfer tube temperature at 250°C. The MS was operated in DDA mode. A scan cycle comprised a full MS scan (m/z range from 335-1800), orbitrap resolution set to 60000, AGC target set to custom, normalised AGC target at 300%, maximum injection time mode set to custom, maximum injection time at 25 ms, microscan set to 1 and source fragmentation disabled. Data of full MS scan were acquired in profile mode. MS survey scan was followed by 20 MS/MS scan events using the following parameters: multiplex ions set to false, isolation window set to 1.4, collision energy mode set to fixed, collision energy type set to normalized, HCD collision energies set to 30%, orbitrap resolution 15000, first mass 110, AGC target set to standard, maximum injection time mode set to custom, maximum injection time set to 40, microscan set to 1. Data for MS/MS DDA scan event were acquired in profile mode. Two blanks were run between each sample to reduce peptide carry-over.

Processing and analysis of proteomics data.   Raw mass spectrometry data files were searched and quantified with the MaxQuant software package (version 1.6.10.43). Proteins and peptides were identified using Uniprot canonical databases. The following search parameters were set: oxidation of methionine and N terminal acetylation were set as variable modifications, carbamidomethylation of cysteine was set as a fixed modification, protein and peptide false discovery rate of 0.01.

In silico determination of carboxyterminal fragment.   Single-pass membrane proteins can be categorized into 4 sub-types (www.uniprot.org), including single-pass type I and type III membrane proteins which both have a N-terminus located at the extracellular side and a C-terminus located at the cytosolic side, and single-pass type II and type IV membrane proteins which have reversed topology. Among all previously identified single-pass membrane γ-secretase substrates (result not shown), 152 out of 156, are single-pass type I membrane proteins. From the four remaining substrates, BCMA,[57] NRADD[84] and SYT7[58] are single-pass type III membrane proteins containing natural short ectodomains. Thus the preferred topology of γ-secretase substrates seems to be N-terminus outside. The fourth one is β 1,6 N-acetylglucosaminyltransferase V (GnT-V)[85] that is the only reported single-pass type II membrane protein to be cleaved by γ-secretase. Only two multi-pass membrane proteins, Glutamate Receptor Subunit 3 (GluR3) and Polycystin-1 (PC1), have been reported to be cleaved by γ-secretase.[86,87] It remains unclear whether these multi-pass proteins become only substrates after cleavage by other enzymes which then generate a single-pass membrane protein fragment, or what exactly is further required to make such proteins a substrate for γ-secretase. Given the complexity of single-pass type II membrane proteins and multi-pass membrane proteins, we focus here only on single-pass type I and III membrane proteins.

The extracellular domain of the CTF that are substrates of γ-secretase are in general less than 50 amino acids (aa) long, while proteins with an extracellular domain larger than 200 aa are not processed by γ-secretase.[21] We used therefore a conservative threshold of 60 aa for the predicted length of the extracellular domain of the γ-secretase substrates, meaning that we considered the part starting from the carboxyl-terminus up to 60 aa beyond the transmembrane domain of the single-pass type I/III membrane protein as theoretical threshold for the determination of the length of the CTF.

Step 5. Spectral pattern visualization of target protein

Data normalization.   We processed the raw intensity values from the proteomics data by a two-step normalization method. Firstly, we normalized every raw intensity value by the sum of raw intensities from the same fraction to rule out the differences possibly caused by loading error of the injection to MS. Then, each value out from the first step normalization was multiplied by the mean fraction weight between two conditions.

Faceted bar plot.   We show the relative abundance of each detected tryptic peptide in a faceted bar plot for each protein separately. The relative abundance of peptides in the 12 fractions were aligned in a row, while the relative abundance of different peptides in the same fraction were aligned in a column. These different rows which show the unique tryptic peptides for each protein are sorted by the location of their first aa residue along the full-length protein. The location of the first aa residue is indicated at the right side of the rows, and are ordered from the amino-terminus down to the carboxyl terminus. The different columns are reflecting the 12 elution batches from left (small) to right (large) molecular weight fractions. We indicate with a double blue line the transmembrane domain (TMD) according to www.uniprot.org, and with a single green line the 60 aa above the double green line which indicates the predicted start of CTF (see *in silico determination of carboxyterminal fragment* under method details section).

Preparation of H9MG single-cell samples

We seeded H9MC collected from D25 as described above in 12-well plates (500,000 cells/well). We grow them in TIC medium for 7 days, TIC medium was refreshed every two days. At Day 7, we pre-treated H9MG with 2 μM Semagacestat or DMSO for 22 h. We added 200 ng/mL LPS or PBS during the last 6 hours of the experiment. For the collection, we added 500 μL Accutase (#07922, Stemcell) with 5 μM Actinomycin D (A1410, Sigma) in each well and incubated the plate at 37 °C for 6 min. We rinsed the cells with cold PBS with 5 μM ActD and collected cells in a clean Eppendorf tube on ice. We spun the cell suspension at 300g for 5min and suspended the cells with cold FACS buffer. We spun down the cell pellets and incubated each of the 12 samples with a specific hashtag antibody (A0251-A0260, A0262 and A0263, Biolegend) at 4 °C. After 30 min, we washed the cells in cold FACS buffer. We spun down the cell pellets again and suspended cells in FACS buffer.

Single-cell mRNA libraries preparation and sequencing
H9MG libraries
We measured the concentration of the cell suspensions on a LUNA cell counter and eventually pooled ∼2,000 cells from each of the 12 samples together (4 conditions: n = 3 samples per condition). We equally divided the pool into 2 and prepared them into 2 cDNA libraries using the 10X Genomics single-cell gene expression profiling kit following the manufacturer's protocol (CG000204_ChromiumNextGEMSingleCell3_v3.1). All cDNA libraries were then sequenced on a DNBSEQ PE100 sequencing platform.
Mouse microglia libraries
We suspended the cells in a final concentration of 1000 cells/μl. We pooled ∼2,000 cells from each of the 3 - 4 samples (each labeled with a specific hashtag antibody, Biolegend) for one cDNA library. For single cell encapsulation, custom microfluidics as described previously[88] was used instead of the standard 10x GEM generation chips. The custom HyDrop chip provided an improved encapsulation efficiency of >75% and better control of droplet formation due to the imaging capabilities of the platform. It helps in preventing the run failure due to chip clogging. The workflow of the HyDrop chip allowed combining two 10x reactions into a single run[88] which enabled us to target for 12000 cell recovery per experimental time point. After single-cell encapsulation, library preparation followed the manufacturer's protocol (CG000204_ChromiumNextGEMSingleCell3_v3.1). All cDNA libraries were then sequenced on a DNBSEQ PE100 sequencing platform.

QUANTIFICATION AND STATISTICAL ANALYSIS

Quantitative analysis of the abundance of the CTFs
Reference plot for calculating molecular weight in the collected fractions
The mean and the 95% confidence interval (CI) of the protein sizes in each fraction was calculated using the data (size and location) from all detected known γ-secretase substrates (See supplementary Table S6). We connected the 95% CIs across all 12 fractions which is the red shadow overlaying part of the reference plot in Figure 1D. By using the reference plots and the predicted size of FL and CTF of each protein, we can deduce the putative location of the FL and CTF of the protein amongst the different fractions, and therefore deduce the location of the green vertical dotted line. For each protein, the peptides derived from the FL protein are in the fractions beyond the vertical green dotted line and the peptides derived from putative CTF fragments are at the left side of that line and below the green horizontal line, so called quadrant 3 or Q3 (see Figures 1C and 1E).
γ-Secretase substrate identification
We quantified the relative total signal in Q3 of the each plot. We consider a protein a substrate of γ-secretase if (1) the increase of CTF upon Semagacestat treatment of the target protein was detected in at least 3 out of 4 independent experiments; (2) the value of Q3 in the Semagacestat treated condition is at least 1.2 fold larger than the value of Q3 in the control condition; (3) P.adj < 0.05, using student t test followed by Benjamini-Hochberg false discovery rate correction, n = 3 or 4.

Functional and Pathway Enrichment Analysis of Candidate Substrates
Candidate substrates identified in the H9MG cells were tested for enrichment of Gene Ontology (GO) Biological Process (BP) and Molecular Function (MF) terms, as well as KEGG pathways, using the clusterProfiler package (v4.2.2). Enriched terms were identified using the *enrichGO()* and *enrichKEGG()* functions, with the parameters qvalueCutoff = 0.05, minGSSize = 100, and pAdjustMethod = "BH". Top GO enrichments were visualized by grouping the 50 most significant terms by semantic similarity, as calculated by the *calculateSimMatrix()* and *reduceSimMatrix()* functions.

Single-cell sequencing data analysis
Alignment, pre-processing, and clustering

H9MG. The 10x Genomics Cell Ranger software (version 6.0.1) was used to align reads to the GRCh38 human reference genome, demultiplex cellular barcodes, and quantify unique molecular identifiers (UMI) and Hashtag oligos (HTO). The UMI and hashtag count matrices for each of the libraries were loaded into the Seurat package (v4.1.1). Genes whose transcripts were identified in less than 3 cells were immediately removed from the expression matrices. Cell barcodes were filtered to include only those detected in both RNA and HTO data. The HTO assays were normalized using the centered log-ratio (CLR) transformation. Seurat's *HTODemux()* function was run with default parameters on the hashtag-count matrices to demultiplex cells into their samples of origin. Cells that could not be assigned to an HTO and cells that were positive for more than one HTO were deemed as negatives and inter-sample doublets, respectively, and removed from further analysis. In the remaining 22,987 demultiplexed singlet, intra-sample doublets were identified and removed using DoubletFinder (v2.0.3). Further quality filtering was performed such that only cells meeting the following cutoffs were retained: < 20% mitochondrial reads, > 5,000 counts, < 65,000 counts, and > 2,000 unique genes. In total, n = 21,851 cells were used for further downstream analysis.

All H9MG single-cell transcriptomes were initially clustered jointly, using Seurat's canonical correlation analysis (CCA) to integrate the RNA transcript counts from the two libraries. In brief, gene counts from each of the libraries were log-normalized for library size and the 2,000 most variable genes were identified using a variance-stabilizing transformation. The *FindIntegrationAnchors()* function was used to identify anchors for the joint dataset and the data was integrated using the *IntegrateData()* function. The integrated data was scaled using *ScaleData()* and a principal component analysis (PCA) was performed with the *RunPCA()* function. Uniform Manifold Approximation and Projection (UMAP) embeddings were created using the *RunUMAP()* function, using the first 29 principal components (PCs) as input for the non-treated cells and 30 PCs for the treated cells (as determined through the visual inspection of a Scree plot). A shared nearest neighbor (SNN) graph was constructed using Seurat's *FindNeighbors()* function, again using 29 and 30 PCs, respectively. Seurat's *AddModuleScore()* function was used to score cells according to their expression of the Friedman proliferating gene set.[54] Cells for which this score was greater than 0 were classified as proliferating. Proliferating cells were removed and the remaining transcriptomes were re-clustered following the above procedure (Figure 4B).

Next, the non-proliferating H9MG transcriptomes were clustered separately depending on the presence or absence of LPS treatment, using the same integration and dimensionality techniques as described in the joint clustering procedure. The UMAP of steady state non-proliferating cells was created using the first 23 PCs and clustered using the same number of PCs, with a resolution of 0.12 (Figure 4D). The UMAP of LPS-treated non-proliferating cells was created and clustered using 15 PCs, with a resolution of 0.15 (Figure 4I).

In vivo microglia. The same alignment and cellular barcode demultiplexing procedures were followed for the *in vivo* microglia harvested from the *C57BL/6J* background (*GS^iΔMG*, *GS^WT*) mice and *App^NL-G-F* background (*App^NL-G-F*-*GS^iΔMG*, *App^NL-G-F*-*GS^WT*, *App^NL-G-F*-Ctrl_QC, and *App^NL-G-F*-TAM_QC) mice. In this instance, reads were aligned to the GRCm38 mouse reference genome. The lincRNAs Gm42418 and AY036118 were removed from the expression matrices, as they overlap a locus that harbors an Rn45s sequence repeat, and may thus obtain inflated expression counts from contaminating 18S rRNA. After demultiplexing cells into samples of origin based on the presence of Hashtag oligos, 9,556 and 46,730 cells were retained from the *C57BL/6J* background mice (n = 8) and *App^NL-G-F* background mice (n = 24), respectively. The cells were further filtered to remove cells with either high/low number of read counts and expressed genes, cells with mitochondrial content > 10%, or intra-sample doublets as identified by DoubletFinder.

For the *C57BL/6J* background mice, the remaining 7,922 single microglia transcriptomes were integrated by library using Seurat's anchor-based integration workflow (as described in the H9MG processing section). The first 20 PCs were used to generate a UMAP and create a SNN graph. The cells were clustered with a resolution of 0.25. Clusters of cells determined to be non-microglial (based on high expression of non-microglial cell-type markers and low expression of microglial markers) and a low-quality cluster (as determined by low UMI counts and high mitochondrial content) were removed. Furthermore, one *GS^iΔMG* sample with a low number of remaining microglial transcriptomes (n = 8) was removed from further analysis. Integration, scaling, and dimensionality reduction was repeated on the remaining 7,285 microglial single cell transcriptomes. 20 dimensions were used for dimensionality reduction. Unbiased clustering by the Louvain algorithm with a resolution of 0.15 identified 4 clusters (Figures 5B and 5C).

For the *App^NL-G-F* background mice, the remaining 41,856 RNA transcript counts (Figure S7A) from three libraries were similarly integrated using integration anchors. The first 26 PCs and a resolution of 0.25 were used to generate a UMAP and cluster the cells (Figure S7B). Non-microglial and low-quality clusters were removed (Figures S7C and S7E). Integration, scaling, and dimensionality reduction was repeated on the remaining 37,884 microglial single cell transcriptomes. 15 dimensions were used for dimensionality reduction. Unbiased clustering by the Louvain algorithm with a resolution of 0.35 identified 9 clusters (Figure S8A). Clusters 0 and 1 were merged, as their marker genes revealed similar homeostatic microglia state profiles (Figures S8B and 6B).

Gene module enrichment visualization

To calculate and visualize the enrichment of gene sets of interest (i.e. markers for microglial states and sets of differentially expressed genes) for each cell, we used Seurat's *AddModuleScore()* function. In brief, this function calculates the activity of a gene set in each cell by comparing the mean abundance level of the genes of interest against the average abundance of sets of random control genes which have a similar average expression level. The calculated scores were visualized on the UMAP. Density plots were created using the Nebulosa package (v1.0.2).

Differential Expression analysis

Differential expressions between clusters and between conditions were performed on the normalized counts using the *FindMarkers()* and *FindAllMarkers()* functions provided within the Seurat package. Min.pct values were set to 0.1. P-values were calculated using the Wilcoxon rank-sum test and were corrected for multiple testing using the Bonferroni method. Seurat's *DotPlot()* and *DoHeatmap()* functions, as well as the ComplexHeatmap package (v1.10.2), were used to visualize the relative expression levels of marker genes on either a per-cell or a per-cluster basis.

Pseudotime analysis

Count matrices and UMAP embeddings were loaded into Monocle 3 (v1.0.0, using SeuratWrappers' *as.cell_data_set()* to convert the Seurat object into a Monocle object. The *learn_graph()* and *order_cells()* functions were used to fit a principal graph, identify trajectories of interest, and assign pseudotime values along the trajectories. Statistical significance of pseudotime values between each of the two conditions being compared was determined using a t-test.

Gene Set Enrichment Analyses

Gene Set Enrichment Analysis (GSEA) was performed using the clusterProfiler package (v4.2.2). The outputs of differential expression analyses between conditions (as obtained by Seurat's *FindMarkers()* function) were ranked according to each gene's signed log_{10}(p-value). clusterProfiler's *GSEA()* function was used to calculated gene set enrichment scores based on the ranked list. The following parameters were used: nPerm = 1000, minGSSize = 10, maxGSSize = 500, pvalueCutoff = 0.05, *pAdjustMethod* = "BH". The enrichments scores of gene sets in the ranked list of differentially expressed genes were visualized using *gseaplot()* function from the enrichPlot package (v1.10.2) (Figures S6C and S6F).

Imaging and quantitative analysis of the Immunofluorescent images

Confocal images were obtained using a Nikon AX Confocal Microscope System driven by NIS-Elements AR (5.41.01) software. For excitation, 405 nm, 488 nm, 561 nm, 640 nm laser lines were used. All the stained sections were imaged by a 4x or 20x objective. Roughly, 8-12 Z-step sections within 15-25 μm thickness were obtained from each sample. All images used for a particular comparative analysis were acquired using the same acquisition parameters. The representative images (in Figure 7H) were processed by FIJI/Image J software using maximum intensity projections of the Z-stack images. The microglia (EYFP$^+$) area, the density of microglial puncta (EYFP$^+$ puncta with diameter > 30 μm), the overlapped microglia and plaque (EYFP$^+$82E1$^+$) area and the total plaque (82E1$^+$) area were quantified using NIS-Elements AR (5.41.01) software. The quantification were performed using a semi-automated house-made macro in NIS-Elements AR software. Briefly, the maximum intensity projections of the Z-stack images were used, and the number of counts and the positive area of either microglia or plaques were identified with threshold function and normalized by the area of interest. All the quantification results were generated using the measurement of the whole cortical region of the brain coronal sections. For all the quantitative analysis, two sections (one anterior section without hippocampus and one posterior section with hippocampus) were randomly selected from each individual animal, stained and imaged as described above. 5 animals in each condition were used for the quantification.

ADDITIONAL RESOURCES

We generated faceted bar-plots of the 359 detected specific single-pass type I and type III membrane proteins from H9MG in this study. The faceted bar-plots are accessible on our website https://data.bdslab.org.